STUDY OF SMALL-SIGNAL STABILITY OF A RENEWABLE INTEGRATED POWER SYSTEM USING A DYNAMIC PHASOR APPROACH

Wasala Appuhamilage Damsith Lakshan

208087L

Degree of Master of Science(Major Component of Research)

Department of Electrical Engineering
Faculty Of Engineering

University of Moratuwa
Sri Lanka

February 2024

STUDY OF SMALL-SIGNAL STABILITY OF A RENEWABLE INTEGRATED POWER SYSTEM USING A DYNAMIC PHASOR APPROACH

Wasala Appuhamilage Damsith Lakshan

208087L

Dissertation submitted in partial fulfillment of the requirements for the degree
Degree of Master of Science(Major Component of Research)

Department of Electrical Engineering
Faculty Of Engineering

University of Moratuwa
Sri Lanka

February 2024

DECLARATION

I declare that this is my own work and this Dissertation does not incorporate without acknowledgement any material previously submitted for a Degree or Diploma in any other University or Institute of higher learning and to the best of my knowledge and belief it does not contain any material previously published or written by another person except where the acknowledgement is made in the text. I retain the right to use this content in whole or part in future works (such as articles or books).

Signature: Date: 18/03/2024

The supervisor should certify the Dissertation with the following declaration.

The above candidate has carried out research for the Degree of Master of Science(Major Component of Research) Dissertation under my supervision. I confirm that the declaration made above by the student is true and correct.

Name of Supervisor: Dr. WD Prasad

Signature of the Supervisor: Date: 18-0302024

DEDICATION

To my devoted parents, whose love, sacrifice, and teachings have been the beacon guiding me through life's journey. To my mother, for her nurturing spirit and unwavering belief in my abilities, and to my father, for his invaluable lessons on perseverance and integrity. And to my cherished wife, who has stood by me as a pillar of strength and understanding throughout this journey. Her love, patience, and encouragement have been the foundation upon which this work was built.

ACKNOWLEDGEMENT

First and foremost, my profound appreciation goes out to Dr. W.D. Prasad from the Department of Electrical Engineering at the University of Moratuwa. His exceptional knowledge, continuous guidance, and relentless support during the course of this research have been invaluable. His commitment to academic excellence and his role as a mentor has consistently motivated me to aim high and tackle challenges with determination and enthusiasm.

In addition, I'd like to express my heartfelt gratitude to the distinguished members of the Department of Electrical Engineering at UOM. Their collective wisdom and support have been pivotal in shaping this work. Moreover, a special acknowledgment is due to the faculty of Electrical and Information Engineering at the University of Ruhuna, where my foundational academic journey commenced. Their teachings and guidance during my undergraduate studies laid the groundwork for the researcher I am today.

ABSTRACT

The transition trend towards renewable energy in the modern world shows a rapid increment of renewable power sources in electrical power systems. Wind energy and solar energy can be considered as the leading energy sources nowadays. These renewable power plants have several power electronic interfaces, and they introduce more complex dynamics to the power system. A comprehensive evaluation is required to identify significant changes in the power system due to these changes. This study provides a detailed examination of the outcomes of introducing renewables to power systems with a significance on its effect on small signal stability and the complex dynamics arising from varying penetration levels of renewable energy sources are explored in-depth, providing a comprehensive understanding of their impact on the stability of the system. This research also revealed the significance of accounting for the network dynamics which are overshadowed in constant admittance network modeling to this study. This research deeply explores the complex mathematical representations of the power system with two types of network modeling techniques and to ensure the accuracy of the model this mathematical model is validated against a nonlinear response. Within this research, attention is drawn to five main scenarios and a real-world case study on wind power integration in Sri Lankan power system.

Keywords: In this research, various concepts and methodologies were explored, focusing on topics such as power system stability, eigenvalue analysis, participation factors, oscillatory modes, renewable energy integration, nonlinear responses, conventional energy sources, dynamic power system models, controller alterations, grid dynamics, power plant influences, wind energy penetration, solar energy penetration, system damping ratios, small signal stability, state matrix, mode shape analysis, complex plane eigenvalues,network interactions

TABLE OF CONTENTS

LIST OF FIGURES

LIST OF TABLES

LIST OF ABBREVIATIONS

Abbreviation	Description
AC	alternating current
DC	direct current
dq	direct quadrature
GSC	Grid side converter
MPPT	Maximum Power Point Tracking
PI	Proportional-Integral
PMSG	permanent magnet synchronous generator
PV	Photovoltaic
RSC	Rotor Side converter
SCIG	squirrel cage induction generators
TSR	Tip Speed Ratio
VSC	voltage source converters
VSI	Voltage Source Inverter
WRIG	wound rotor induction generators

LIST OF APPENDICES

CHAPTER 1

INTRODUCTION

1.1 Power System Stability

Power system stability refers to the ability of a power system, for a given initial operation condition, to regain a state of operating equilibrium after being subjected to a disturbance and ensuring that steady state and transient operating conditions are within acceptable limits (1). As shown in figure 1.1 Power system stability considers five key areas: resonance stability, converter driven stability, rotor angle, frequency, and voltage stability. Rotor angle stability is about keeping generators in synchronous operation, especially after disturbances. It can be further split into two main categories (2). Firstly, there's transient stability (large disturbance), gauging the system's resilience to significant disturbances such as faults, switch operations, and sudden power source loss. Secondly, small signal stability (small continuous disturbance), focuses the small continuous disturbances such as load fluctuations, mechanical oscillations of generators, variations in renewable generation, etc. Frequency stability evaluates the system's ability to maintain a constant frequency, especially if the generation and the consumption of power aren't perfectly balanced. Voltage stability ensures that the power system maintains the right voltage levels. This involves both short-term and long-term. Short-term voltage stability is associated with the dynamics of fast-acting loads and their effect on the transmission system while long-term voltage stability is related to the slower-acting devices such as tap-changing transformers and generator voltage regulators and how they interact with increasing demand (1).

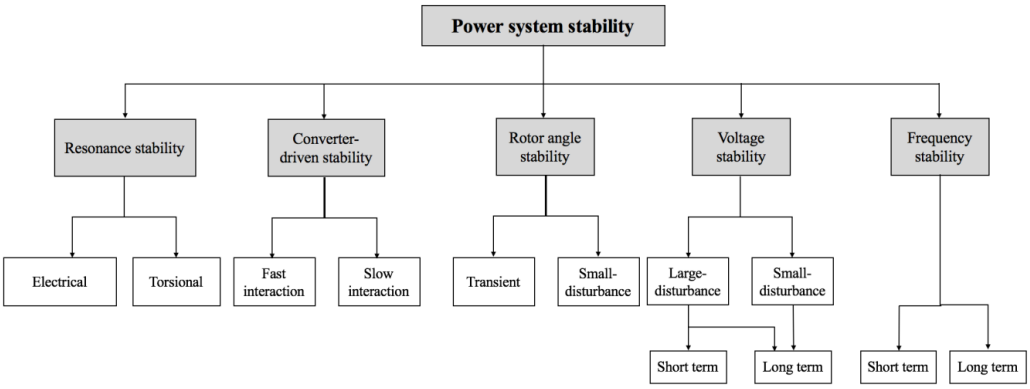

Fig. 1.1. *Classification of Power System Stability*

1.2 Small Signal Stability

The small signal stability is one of the most important factors in power system operation. Small signal stability is the ability of the power system to maintain synchronous operation subsequent to a small disturbance. The power system with poor small-signal stability can experience sustained oscillations these oscillations start small but they can grow in magnitude, and they have the potential to lead the power system to operational challenges like protective relay tripping, voltage, and frequent variations and specifically affect the grid reliability.(3)

With the integration of more renewable sources such as solar power and wind power into the power grid more complex dynamics are introduced because these renewables have a number of power electronic interfaces like converters, controllers, etc. These dynamics can affect negatively on the power system so the small signal stability plays a significant role here. Most conventional power plants consist of synchronous generators and those generators provide a significant amount of inertia to the system to damp out oscillations and help the system maintain synchronism.However renewable power plants such as solar power plants and wind power plants do not directly contribute to the system inertia in same way. So, replacing conventional power plants with renewable power plants can reduce the inertia of the system, make the power system more sensitive to disturbances, and lead to faster and less damped oscillations. The change is exacerbated by the controllers in wind and solar plants, which, while optimizing outputs, can interact with other grid controllers, creating unforeseen oscillatory interactions. It is necessary to assess the small signal stability of the power system with the integration of various levels of renewable power.(3)

Small signal stability analysis is essential in power systems engineering as it provides valuable insights into the dynamic behavior of the system under small disturbances as described above. While tools like PSCAD and PSSE are proficient in simulating transient and steady-state conditions, they may not capture the intricate details of small signal stability adequately. Small signal stability analysis focuses on the linearized behavior around an operating point, allowing engineers to assess the system's response to small disturbances such as fluctuations in load or renewable energy sources. By examining the eigenvalues and mode shapes of the linearized system, engineers can identify critical modes that may lead to oscillations or instability. This analysis aids in designing effective control strategies and ensuring the overall stability of the power system, complementing the capabilities of tools like PSCAD and PSSE by offering a more detailed understanding of system dynamics under small perturbations.

1.3 Analyzing Small Signal Stability Through Linearization

To analyze small signal stability, the system is linearized around a certain operating point. The eigenvalues of the sate matrix (Jacobian matrix) of the system are used to analyze the system. An eigenvalue of a matrix A is a scaler λ such that when A is multiplied by a non-zero vector v, the result is a scaler multiple of v as (1.1).

$$Av = \lambda v \tag{1.1}$$

Where:

- A is the matrix.
- v is the eigenvector of A associated with the eigenvalue λ.
- λ is the eigenvalue.

For each eigenvalue λ, there might be one or more associated eigenvectors. The process of determining the eigenvalues of a matrix involves solving the characteristic polynomial:

$$\det(A - \lambda I) = 0$$

Where:

- det represents the determinant.
- I is the identity matrix of the same size as A.

The roots of this polynomial equation give the eigenvalues λ of the matrix A. Once the eigenvalues are known, the corresponding eigenvectors can be determined by plugging each eigenvalue into the following equation(1.2) and solving for v.

$$(A - \lambda I)v = 0 \tag{1.2}$$

The real parts of the eigenvalues of the state matrix dictate the stability of the system. If all the eigenvalues have negative real parts, the system is stable but if any eigenvalue has a positive real part means the system is unstable. Participation factors are used to identify which state of the system most influences a particular eigenvalue or mode and it is calculated by using the corresponding eigenvector of that eigenvalue.Given the linearized model of a power system, the participation factor P_{ij} of the i^{th} state in the j^{th} mode is computed as:

$$P_{ij} = \frac{|\phi_{ij}|^2}{\sum_k |\phi_{kj}|^2} \tag{1.3}$$

where ϕ_{ij} is the element of the eigenvector corresponding to the i^{th} state and j^{th} mode. The denominator represents the summation of the squares of the magnitudes of all elements in the j^{th} eigenvector. The eigenvalues' real and imaginary parts are used to determine the damping ratios of the oscillatory modes, which give insights into how quickly disturbances die out. A lower damping ratio might indicate potential stability concerns. Given complex mode $\lambda = \sigma \pm j\omega$ which represents an oscillatory mode, the frequency and the damping ratio can be computed as follows:

Frequency f is given by (1.4):

$$f = \frac{\omega}{2\pi} \tag{1.4}$$

Damping ratio D is calculated as (1.5):

$$D = 100 \times \frac{-\sigma}{\sqrt{\sigma^2 + \omega^2}} \tag{1.5}$$

The small signal stability study of a power system is performed by linearizing the dynamic equations of that power system's mathematical model around a steady-state operating point. Because of that the accuracy of the small signal stability analysis mainly depends on the accuracy of the power system model used in the study[1]. As an example, when the constant admittance representation is used to model the network may not detect any interaction from the network to the system stability. Although, when the dynamic phasor network representation is used to model the network the network dynamics are also taken in to account. (3)

1.4 Wind Power Plants

With the world's transition towards sustainable energy, the utilization of wind power plants has significantly grown in recent years. Due to the low generation cost and the cleanness of wind power, many countries in the world are now investing in wind power plants. As per the records wind energy sources accounted for nearly 7.33 percent of electricity generation worldwide in 2022, up from a 6.6 percent share a year earlier(4). By considering the operation arrangement and the turbine technology, wind power plants are mainly divided into main 4 categories as shown in the figure (1.2)(5).

Type 1, Fixed-Speed Induction Generators (FSIG)

- Fixed speed turbines are used.
- Typically uses squirrel cage induction generators (SCIG) .
- Directly connected to the grid without any power electronic converter.
- Blades are fixed at a specific angle and this design lacks flexibility in adapting to varying wind speeds.

Type 2, Limited Variable Speed Wind Turbines

- Variable-speed turbines with limited speed ranges are used.
- Typically uses wound rotor induction generators (WRIG) with variable resistor banks on the rotor side.
- Provide some flexibility in adapting to wind changes but lacks full-scale power electronic converters for more adaptable speed range.

Type 3, Doubly Fed Induction Generators (DFIG)

- Variable-speed wind turbines are used.
- Uses a wound rotor induction generator, with the rotor connected to the grids through slip rings and a partial scale power electronic converter.
- This allows for a wide range of operational speeds, improving efficiency under varying wind conditions.

Type 4, Full-Scale Converter Wind Turbines

- Fully variable-speed turbines are used.
- Typically, Permanent magnet synchronous generators or electrically excited synchronous generators are used but other types are also available.
- The generator is decoupled from the grid using a full-scale power electronic converter. This type is the most flexible and adaptable to wind speed variations and variable grid conditions.

1.5 Solar power plants

As global trends shift towards green energy, solar power has experienced a significant surge in adoption, establishing itself as a crucial component in the global energy mix. Solar power plants capture sunlight and convert it into electricity and offer environmentally friendly electricity generation. The most common type of solar power plant is Photovoltaic (PV) solar plant (6). These PV cells directly convert sunlight into electricity. There are some other types of power plants as Concentrated solar power plants, Solar hybrid power plants, etc. Solar power plants are integrated into the grid via a well-coordinated power electronic system. Solar panel direct current (DC) output is transferred to alternating current (AC) output by the inverter as shown in figure (1.3) in order to make grid compatibility (7).

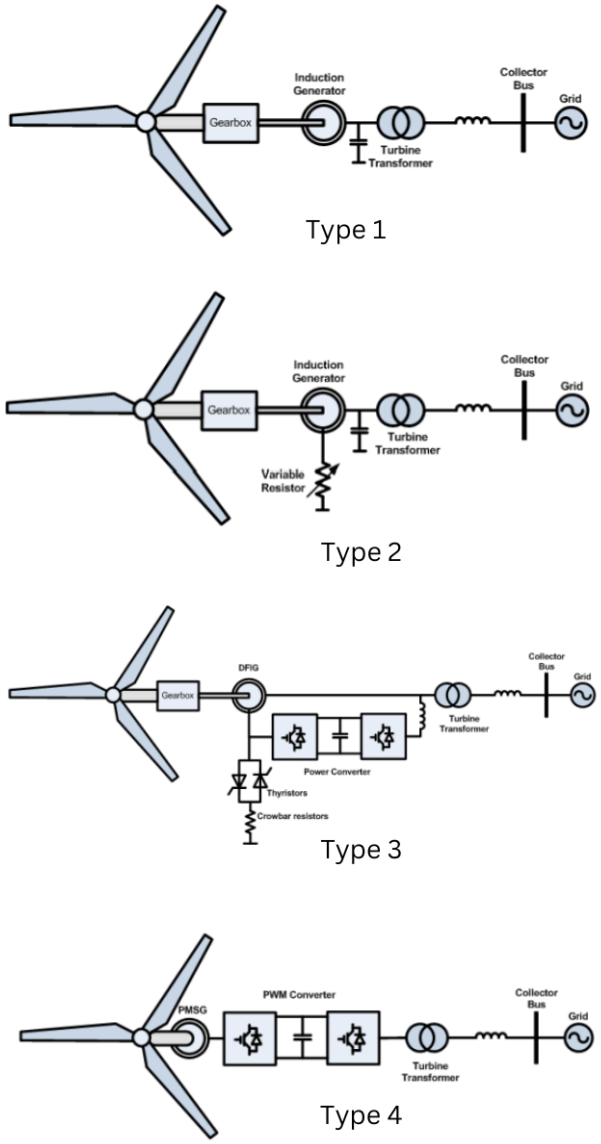

Fig. 1.2. *Different types of wind turbine generators*

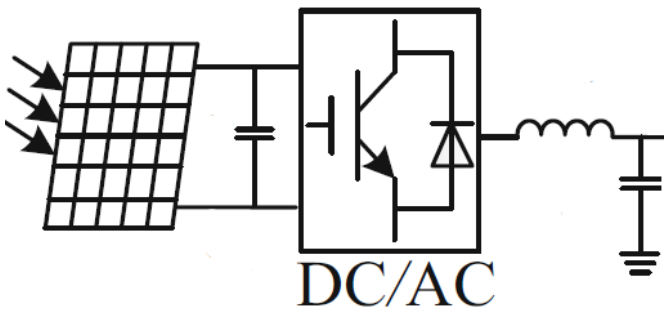

Fig. 1.3. *Configuration of PV generation*

1.6 Objective Of The Study

With the recent trend towards renewable power in the world, the power sector is experiencing a surge of renewable power plants (such as wind power and solar power) integration into the power grid. As explained in previous sections, adding more renewable power plants to the system can impact the system's overall dynamics and cause considerable shifts in stability. So, to maintain proper operation in the power system, small signal stability studies become more important.

The primary objective of this study is to perform a small-signal stability assessment of a power system with and without non-conventional renewable-based energy generation and conduct an investigation on the impact and the damping characteristic of dominant oscillation in the system under different system conditions such as integration of different power plant types (conventional + renewable) and in different penetration levels of renewable power plants.

The accuracy of the small signal stability analysis is mainly related to the accuracy of the power system model used since these stability studies are embedded around linearizing the dynamic equations of the power system model relative to a steady state operation point. Under power system modeling the main attention goes to the power plant modeling and the network modeling. There are several network modeling techniques to use in power system modeling such as constant admittance network representation, detail representation, and Dynamic phasor representation. In this study, those techniques are reviewed to identify the most suitable network modeling technique for optimal results.

In this research, main five scenarios, starting from one that uses only conventional sources to others that incorporate renewables (wind and solar) are carefully chosen to understand the behavior of the power system's small signal stability with the integration of renewables, and those scenarios are designed to explore unique combinations of conventional and non-conventional power sources and their interplay within the network. Among those scenarios, the scenario with only conventional sources is chosen as the benchmark of the study.

Apart from the above-described five scenarios, a key aspect of this research will focus on the Sri Lankan power system. This part of the study will deeply assess the small-signal stability within this power system at two distinct voltage levels: 220kV and 132kV with and without the Mannar wind power plant. This aims to analyze the stability of the Sri Lankan power system when it is after continuous small disturbances and the repercussions of integrating the Mannar Wind power plant into the Sri Lankan power system on its small signal stability.

1.7 Organization Of The Thesis

the thesis is structured into four main chapters to provide a cohesive exploration of small signal stability in power systems with renewable integrations:

1. **Chapter 1: Introduction**
    - Introduces the concepts of power system stability and the role of wind and solar power plants, and establishes the study's objectives.
2. **Chapter 2: Mathematical Models of Power System Elements**
    - Focuses on the modeling of power system elements, detailing both conventional and renewable power plants. This chapter also elaborates on network modeling approaches and introduces various test scenarios.
3. **Chapter 3: Results and Analysis**
    - Presents the outcomes of the proposed models across different scenarios, emphasizing the implications on system stability. A summary of key findings concludes this chapter.
4. **Chapter 4: Conclusion**
    - Offers a conclusion of the entire study, encapsulating major findings and their implications.

CHAPTER 2

MATHEMATICAL MODELING OF POWER SYSTEMS FOR SMALL SIGNAL STABILITY ASSESSMENTS

Mathematical modeling serves as the foundation for small signal stability analysis. Models of system components, such as generators, transmission lines, loads, transformers, control systems, and power electronic components, capture the behavior of these elements for analytical purposes. In this context, the electrical power system is described by a combination of differential and algebraic equations. This analysis primarily focuses on components like conventional power plants, wind and solar power plants, loads, and the transmission network. This section delves into the modeling of each power system component and the formulation of their respective linear models.

2.1 Power Plant Modeling

Mathematical modeling of power plants is essential for capturing their dynamic behaviors. Under this section, three types of power plants are modeled.

2.1.1 Conventional Power Plant Modeling

Synchronous generators are the most common type of generators used in conventional power plants and it is the main energy source of a power plant. The equivalent circuit of a synchronous generator is shown in figure 2.1. Synchronous generators are mainly classified into two categories, namely the Salient pole and the Round rotor. They can be represented by using seven and eight dynamic equations respectively, including stator transients which are known as the 7^{th} order model and the 8^{th} order model. This 8^{th} order model can be simplified to 7^{th} order model by removing the second damper winding in the q axis. In 7th order model the eqution (2.8) is not present. Equations (2.1) to (2.8) shows the dynamic equations of a synchronous generator.(3)

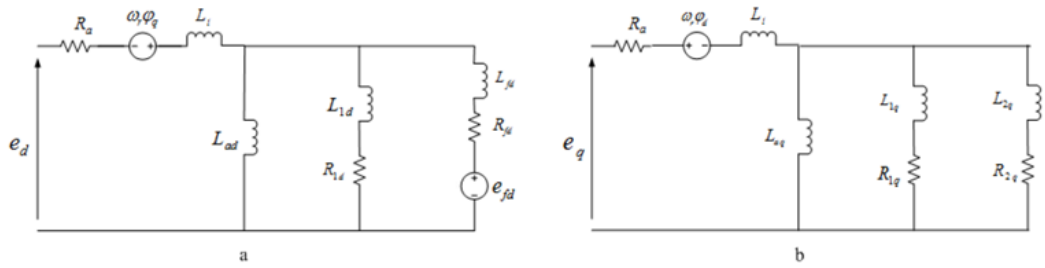

Fig. 2.1. *Synchronous generator equivalent circuit in d-q frame*

$$\Delta\dot{\delta}_r = \omega_0 \Delta\omega_r \tag{2.1}$$

$$\Delta\dot{\omega}_r = \frac{1}{2H}\left(T_m - T_e - K_D\frac{d\delta_r}{dt}\right) \tag{2.2}$$

$$\dot{\psi}_d = \omega_0\left(e_d + \psi_q\omega_r + R_a i_d\right) \tag{2.3}$$

$$\dot{\psi}_{fd} = \omega_0\left(e_{fd} + \frac{(\psi_{ad} - \psi_{fd})R_{fd}}{L_{fd}}\right) \tag{2.4}$$

$$\dot{\psi}_{1d} = \omega_0\frac{(\psi_{ad} - \psi_{1d})R_{fd}}{L_{fd}} \tag{2.5}$$

$$\dot{\psi}_q = \omega_0\left(e_q - \psi_d\omega_r + R_a i_q\right) \tag{2.6}$$

$$\dot{\psi}_{1q} = \omega_0\frac{(\psi_{aq} - \psi_{1q})R_{1q}}{L_{1q}} \tag{2.7}$$

$$\dot{\psi}_{2q} = \omega_0\frac{(\psi_{aq} - \psi_{2q})R_{2q}}{L_{2q}} \tag{2.8}$$

The corresponding linearized state equations of an 8$^{\text{th}}$ order synchronous generator are shown in (2.9).

$$\Delta\dot{X}_g = A_g\Delta X_g + B_g\Delta U_g + E_g\Delta I_g \tag{2.9}$$

$$\Delta X_g = \begin{bmatrix}\Delta\omega_r & \Delta\delta_r & \Delta\Psi_d & \Delta\Psi_{fd} & \Delta\Psi_{1d} & \Delta\Psi_q & \Delta\Psi_{1q} & \Delta\Psi_{2q}\end{bmatrix}^T$$

$$\Delta U_g = \begin{bmatrix}\Delta T_m & \Delta E_{fd}\end{bmatrix}^T$$

$$\Delta I_g = \begin{bmatrix}\Delta I_R & \Delta I_I\end{bmatrix}^T$$

Here $\Delta\omega_r$, $\Delta\delta_r$ are speed deviation and the rotor angle deviation of the rotor. $\Delta\Psi_d$, $\Delta\Psi_q$ are deviation of d-axis and q-axis stator fluxes. $\Delta\Psi_{fd}$ is field winding flux deviation. $\Delta\Psi_{1d}$, $\Delta\Psi_{1q}$, $\Delta\Psi_{2q}$ are the deviations of the flux of damper winding 1 and 2. ΔE_{fd}, ΔT_m are the field voltage and mechanical torque deviations respectively. ΔI_R and ΔI_I are the terminal currents in the R-I reference frame.

Conventional power plants are equipped not only with synchronous generators but also with auxiliary control systems like exciter, governors, etc. The exciter controls the voltage by adjusting the current to the synchronous generator's field windings while the governor stabilizes the turbine speed and manages output by modulating the flow, ensuring consistent and effective operation. The turbine converts energy from the fluid flow to mechanical energy which drives the generator.

In this study, the synchronous generator was considered to be provided with an IEEE AC4A exciter. The control block diagram of the simplified version of the exciter is shown in Fig. 2.2 and all the dynamic equations are as shown from equation (2.10) to (2.13) and the related state equations are shown in (2.14). In this exciter model, T_1, T_B, T_A, T_E are time constants; ΔV,ΔV_{ref} are the deviations of the generator terminal voltage and the exciter reference voltage respectively. State variables X_1 and X_2 were selected as shown in Fig. 2.2. ΔV_R and ΔV_I are the generator terminal voltage in R-I reference frame.

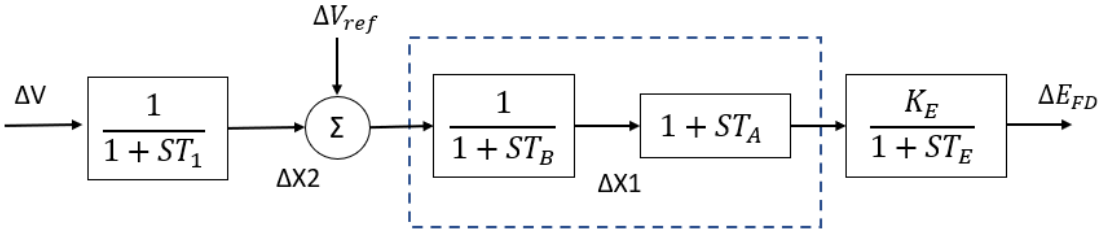

Fig. 2.2. *AC4A exciter control block diagram*

$$\Delta \dot{E}_{fd} = \frac{K_E}{T_E}\Delta X_1 + \frac{K_E T_A}{T_E}\Delta \dot{X}_1 - \frac{1}{T_A}\Delta E_{fd} \tag{2.10}$$

$$\Delta \dot{X}_1 = -\frac{1}{T_B}\Delta X_2 + \frac{1}{T_B}\Delta V_{\text{ref}} - \frac{1}{T_B}\Delta X_1 \tag{2.11}$$

$$\Delta \dot{X}_2 = \frac{1}{T_1}\Delta V - \frac{1}{T_1}\Delta X_2 \tag{2.12}$$

$$\Delta V = \frac{\Delta V_R}{|E_t|} + \frac{\Delta V_I}{|E_t|} \tag{2.13}$$

$$\Delta \dot{X}_e = A_e \Delta X_e + B_e \Delta U_e + E_e \Delta V_e \tag{2.14}$$

Here,

$$\Delta X_e = [\Delta E_{fd} \quad \Delta X_1 \quad \Delta X_2]^T$$

$$\Delta U_e = \Delta V_{ref}$$

$$\Delta V_e = [\Delta V_R \quad \Delta V_I]^T$$

For this analysis, the combined governor-turbine model is used as shown in figure 2.3 and it would integrate the effect of the governor's control action with the dynamic response of the turbine to those actions. When combined, their dynamics give the overall response of the generation to frequency deviations. The dynamic equations for this model is shown in equation (2.15) to (2.20) .

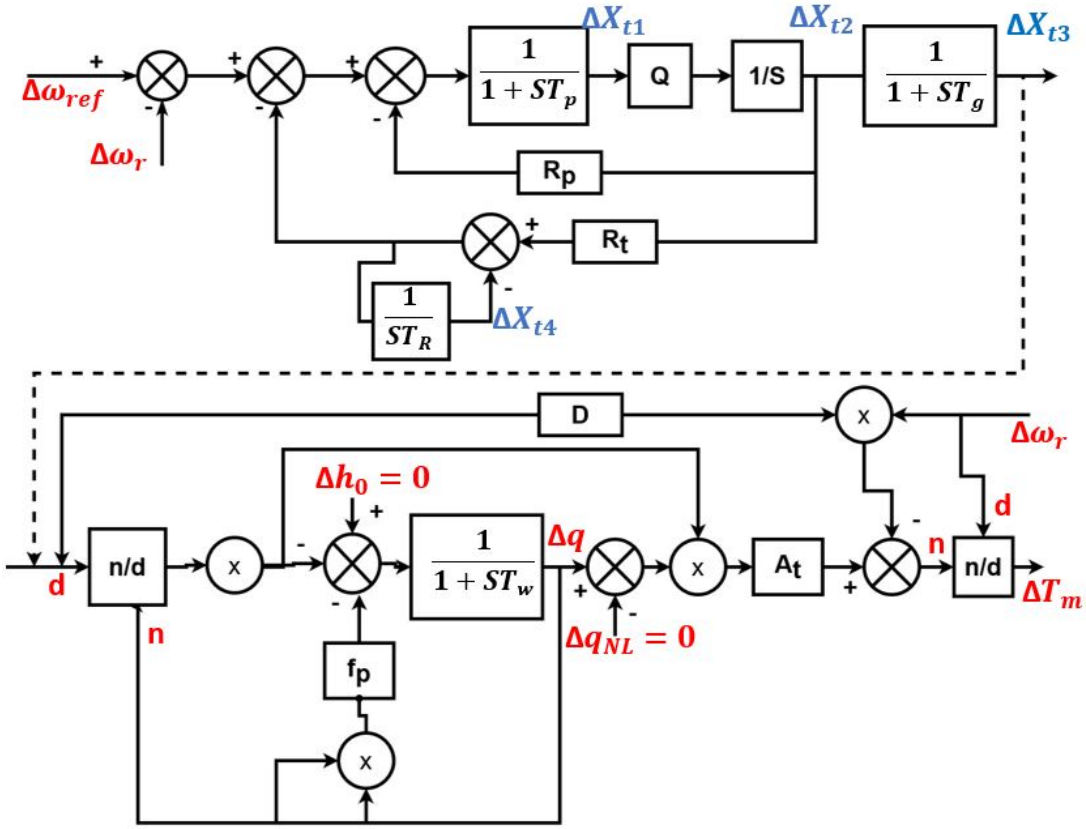

Fig. 2.3. *Governor-Turbine block diagram*

$$\Delta\dot{X}_{t1} = -\frac{1}{T_p}\Delta X_{t1} + \frac{-R_t + R_p}{T_E}\Delta X_{t2} - \frac{1}{T_P}\Delta X_{t4} - \frac{1}{T_p}\Delta\omega_r + \frac{1}{T_p}\Delta\omega_{\text{ref}} \tag{2.15}$$

$$\Delta\dot{X}_{t2} = Q\Delta X_{t1} \tag{2.16}$$

$$\Delta\dot{X}_{t3} = \frac{1}{T_g}\Delta X_{t2} - \frac{1}{T_g}\Delta X_{t3} \tag{2.17}$$

$$\Delta\dot{X}_{t4} = \frac{R_t}{T_R}\Delta X_{t2} - \frac{1}{T_R}\Delta X_{t4} \tag{2.18}$$

$$\Delta\dot{q} = \frac{2q^2}{T_w G^3}\Delta X_{t3} - \frac{2q}{T_w}\left[\frac{1}{G^2} - f_p\right]\Delta q \tag{2.19}$$

$$\Delta T_m = -\frac{2A_t q^2}{G^3}[q - q_{NL}]\Delta X_{t3} + \frac{A_t}{G^2}[3q^2 - 2q_{NL}q]\Delta q - \left[DG + \frac{A_t q^2}{G^2}[q - q_{NL}]\right]\Delta\omega_r \tag{2.20}$$

Here, ΔT_m typically represents the deviation or change in mechanical torque. q denotes the flow deviation, while q_{NL} signifies the reference flow. T_p, T_E, T_P, T_g, T_R, and T_w are time constants. ω_r represents the deviation in rotor speed from its nominal value, and ω_{ref} is the reference speed. The corresponding state equation for the governor and the turbine model is shown bellow equation (2.21).

$$\Delta \dot{X}_t = A_t \Delta X_t + A^1{}_t \Delta \omega_r + B_t \Delta U_t \tag{2.21}$$

$$\Delta X_t = [\Delta X_{t1} \quad \Delta X_{t2} \quad \Delta X_{t3} \quad \Delta X_{t4} \quad \Delta q]^T$$

$$\Delta U_t = \Delta \omega_{ref}$$

(2.21).

$$\Delta \dot{T_m} = A_m \Delta X_t + B_m \Delta \omega_r \tag{2.22}$$

The overall state-space model for a conventional power plant can be represented as follows.

$$\begin{bmatrix} \Delta \dot{X}_g \\ \Delta \dot{X}_e \\ \Delta \dot{X}_t \end{bmatrix} = A_G \begin{bmatrix} \Delta X_g \\ \Delta X_e \\ \Delta X_t \end{bmatrix} + B_G \begin{bmatrix} \Delta \omega_r \\ \Delta V_{\text{ref}} \end{bmatrix} + E_G \begin{bmatrix} \Delta V_R \\ \Delta V_I \end{bmatrix} \tag{2.23}$$

$$\begin{bmatrix} \Delta \dot{I}_g \end{bmatrix} = C_G \begin{bmatrix} \Delta X_g \\ \Delta X_e \\ \Delta X_t \end{bmatrix} \tag{2.24}$$

2.1.2 Wind Power Plant Modeling

Among the various types of wind turbine configurations, the Type 4, or full converter wind turbine presents unique changes in modeling due to the existence of a power electronic converter that decouples the generator from the grid. The main parts of the type 4 wind power plant are shown in figure 2.4. The turbine of the wind power plant absorbs energy from wind and transfers it in to a permanent magnet synchronous generator (PMSG) through a gearbox. This gearbox plays a pivotal role in adjusting the rotational speed of the turbine blades to match the optimal operating speed of the PMSG. The PMSG produces AC and that power flows into a rectifier, converting it to DC. This DC output is then stabilized using a DC link capacitor, ensuring a consistent and smooth voltage level. Subsequently, this DC voltage is fed into a network-side inverter, which transforms it back to AC, suitable for grid transmission. Before being dispatched to the grid, a step-up transformer is employed to adjust this AC voltage to the grid's requisite level. This entire arrangement not only ensures efficient power conversion but also provides the flexibility to manage grid disturbances and integrate seamlessly with other energy sources (5). After extensively reviewing previous research in wind power generation, it's clear that certain key components form the foundation of today's

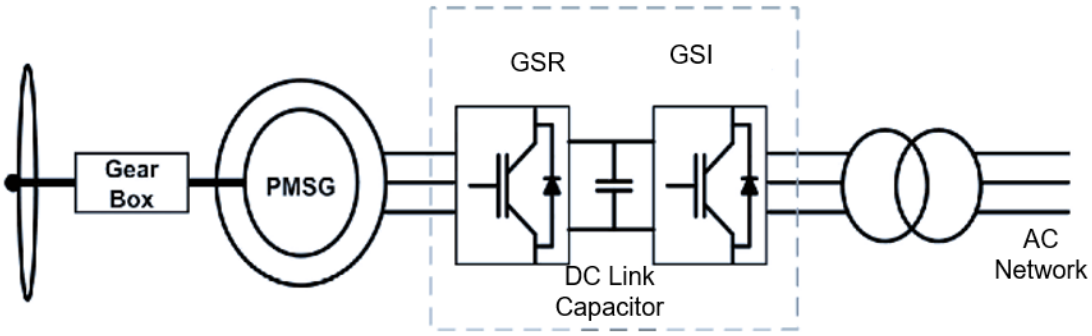

Fig. 2.4. *Typical components of a type 4 wind turbine*

wind power plants. They include:

- Wind Turbine
- Drive Train
- Permanent Magnet Synchronous Generator
- Generator Side Rectifier
- DC Link
- Voltage Source Inverter (VSI)

2.1.2.1 Wind Turbine Model

The power harnessed from a wind turbine is often described by the equation (2.25):

$$P_w = 0.5\pi\rho R^2 C_p V_w^3 \tag{2.25}$$

In the given equation, P_w denotes the power extracted from the wind, ρ represents the air density, R is the radius of the turbine blades with πR^2 indicating the swept area, C_p serves as the power coefficient indicative of the turbine's efficiency, and V_w stands for the wind speed. The performance coefficient, symbolized as C_p, is intricately associated with two primary parameters: the Tip Speed Ratio (TSR) , denoted by λ, and the pitch angle, represented as β. The Betz limit, a foundational concept in wind energy science, postulates a maximum attainable efficiency of 59.3% for any wind turbine. However, real-world scenarios, especially in commercial turbines, typically exhibit a C_p ranging between 20% and 45% (8).The TSR is defined by the equation (2.26):

$$\lambda = \frac{\omega_r \times R}{V_w} \tag{2.26}$$

2.1.2.2 Drive Train Model

The drive train of a wind turbine can be conceptualized using various models: the one-mass model, the two-mass model, and the three-mass model. In the one-mass model, components such as the generator, turbine hub, and blades are amalgamated into a single consolidated mass. The two-mass model differentiates between the wind turbine and the generator, viewing them as two distinct masses linked by a flexible shaft. The Three Mass Model further segments the system, considering the flexible segment of the blade as one mass, the turbine hub combined with the rigid section of the blade as another, and the generator as the third distinct mass (9).

Given the intricacies and granularity offered by these models, this study has adopted the two mass drive train model, illustrated in Fig.2.5. In this representation, J_1 and J_2 symbolize the moments of inertia for the blades and the generator, respectively. Damping for these components is represented by D_1 and D_2. K_{12} denotes the stiffness coefficient bridging the blade and generator, while D_{12} signifies the damping coefficient between them.

The two-mass model of the PMSG wind turbine showcased in Fig. 2.5, is rooted in both Hook's law and Newton's Second law and can be expressed by using the following dynamic equations from (2.27) to (2.30). The linearized state equations for the drive train are shown in equation (2.31).

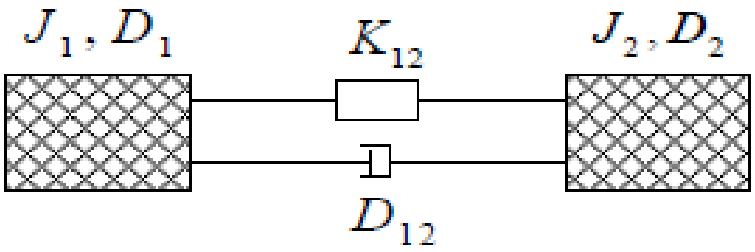

Fig. 2.5. *Drive train two mass model*

$$\Delta\theta_1 = \Delta\dot{\omega}_1 \tag{2.27}$$

$$\Delta\theta_2 = \Delta\dot{\omega}_2 \tag{2.28}$$

$$J_1\Delta\dot{\omega}_1 = \Delta T_w - D_1\Delta\omega_1 - D_{12}(\Delta\omega_1 - \Delta\omega_2) - K_{12}(\Delta\theta_1 - \Delta\theta_2) \tag{2.29}$$

$$J_2\Delta\dot{\omega}_2 = \Delta T_e - D_2\Delta\omega_2 - D_{12}(\Delta\omega_2 - \Delta\omega_1) - K_{12}(\Delta\theta_2 - \Delta\theta_1) \tag{2.30}$$

Where: T_w represents the aerodynamic torque from the wind turbine, T_e denotes the electro-mechanical torque from the generator. The terms J_1 and J_2 refer to the moments of inertia for the blades and the generator rotor, respectively. D_1 and D_2 describe the damping values for the blades and generator rotor, respectively. K_{12} stands for the stiffness coefficient between the blade and generator rotor, and D_{12} is the damping

coefficient acting between the blade and generator rotor.

$$\Delta \dot{X}_{dt} = A_{dt}\Delta X_{dt} + B_{dt}\Delta U_{dt} \tag{2.31}$$

$$\Delta X_{dt} = [\Delta\Theta_1 \quad \Delta\Theta_1 \quad \Delta\omega_1 \quad \Delta\omega_2]^T$$

$$\Delta U_{dt} = [\Delta T_w \quad \Delta T_e]^T$$

2.1.2.3 Permanent Magnet Synchronous Generator Model

The PMSG plays a pivotal role in tapping wind energy, transforming the mechanical power gleaned from the wind turbine into usable electrical energy. It is frequently used in wind turbine applications due to its advantages like high efficiency and the absence of a need for external excitation.

Modeling the PMSG involves capturing its electrical dynamics, magnetic properties, and its interaction with connected systems. The PMSG can be described in both the direct quadrature (dq) frame of reference as shown in figure 2.6 and the abc (phase) frame. The dq model is more commonly used as it simplifies the analysis for control and understanding of the generator's behavior under various conditions(10)(11).

The basic dynamic equations of a PMSG in the dq frame can be represented as:

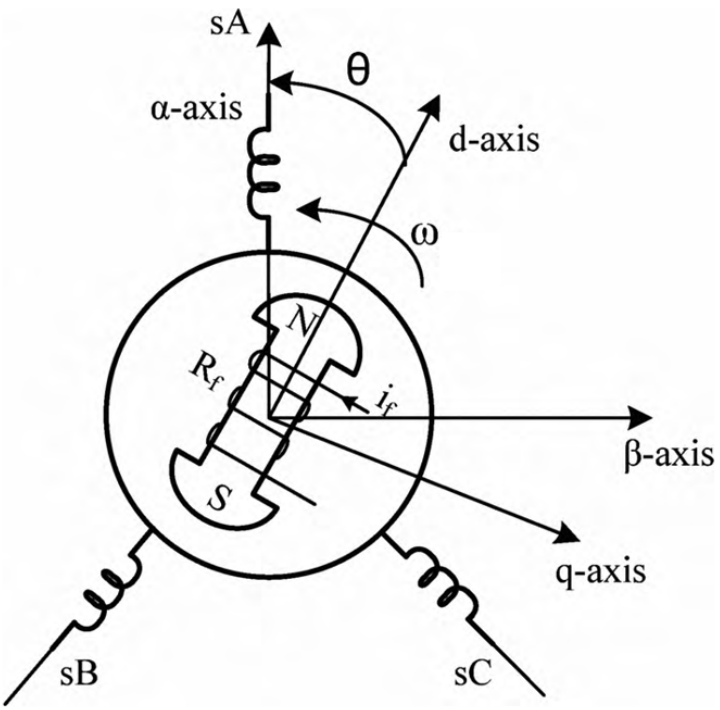

Fig. 2.6. *PMSG d-q axis representation*

$$V_{ds} = -Ri_{ds} - \omega_r\psi_{qs} + \dot{\psi}_{ds} \tag{2.32}$$

$$V_{qs} = -Ri_{qs} + \omega_r \psi_{ds} + \dot{\psi_{qs}} \tag{2.33}$$

The flux linkage can be written as,

$$\psi_{ds} = -L_{ds} i_{ds} + \psi_{rd} \tag{2.34}$$

$$\psi_{qs} = -L_{qs} i_{qs} + \psi_{rq} \tag{2.35}$$

$$\psi_{rd} = \psi_{PM} \tag{2.36}$$

$$\psi_{rq} = 0 \tag{2.37}$$

Where n_p denotes the pole pairs. The inductances of stator windings against the d-axis and q-axis are represented by L_d and L_q, respectively. Similarly, i_d and i_q refer to the currents of the stator windings against the respective d-axis and q-axis. The flux linkage of the rotating magnet is captured by ψ_{PM}, while the flux linkages of the rotor windings against the d-axis and q-axis are symbolized by ψ_{rd} and ψ_{rq}. Lastly, ψ_{ds} and ψ_{qs} describe the flux linkages of the stator windings in the d-axis and q-axis, respectively.By linearizing the above equations, we can structure them into the following format as in equation (2.38).

$$\begin{aligned} \Delta \dot{X_{pm}} &= A_{pm} \Delta X_{pm} + B_{pm} \Delta U_{pm} \\ \Delta X_{pm} &= [\Delta \Psi_{ds} \quad \Delta \Psi_{ds}]^T \\ \Delta U_{pm} &= [\Delta V_{ds} \quad \Delta V_{qs} \quad \Delta \omega_2]^T \end{aligned} \tag{2.38}$$

2.1.2.4 Rotor Side Converter

Full-scale back-to-back PWM converter systems are frequently equipped with PMSGs, celebrated for their impressive fault ride-through capabilities and robust grid voltage support. A typical configuration of such a system includes a wind turbine, a PMSG, and two voltage source converters (VSC) . The two VSCs are typically distinguished as the Rotor Side converter (RSC) , which functions as a rectifier, and the Grid side converter (GSC) , which operates as an inverter. Within the operational strategies for GSCs, the decoupled d-q vector control and power signal feedback control stand out as the dominant control schemes. This study has used the power signal feedback control approach for the RSC (12).

The power signal feedback control scheme is designed to maximize the efficiency and responsiveness of wind energy conversion systems. This control method leverages real-time power measurements to ensure optimal power extraction from the wind. The system constantly monitors the actual power output of the turbine and compares it against the desired or reference power, typically set by Maximum Power Point Tracking (MPPT) algorithms. The resulting error signal, derived from this comparison, is

then processed using controllers, often of the Proportional-Integral (PI) type, to adjust the operational parameters of the turbine, ensuring it continually operates at its most efficient point. This feedback loop not only ensures maximum power extraction under varying wind conditions but also helps in achieving grid compatibility by providing enhanced voltage and frequency support. The agility and adaptability of the power signal feedback control scheme make it particularly suitable for wind energy systems, which are inherently subject to fluctuating wind speeds and directions. Figure 2.7 shows the block diagram of the RSC and the dynamic equations are shown from equation (2.39) to (2.42).

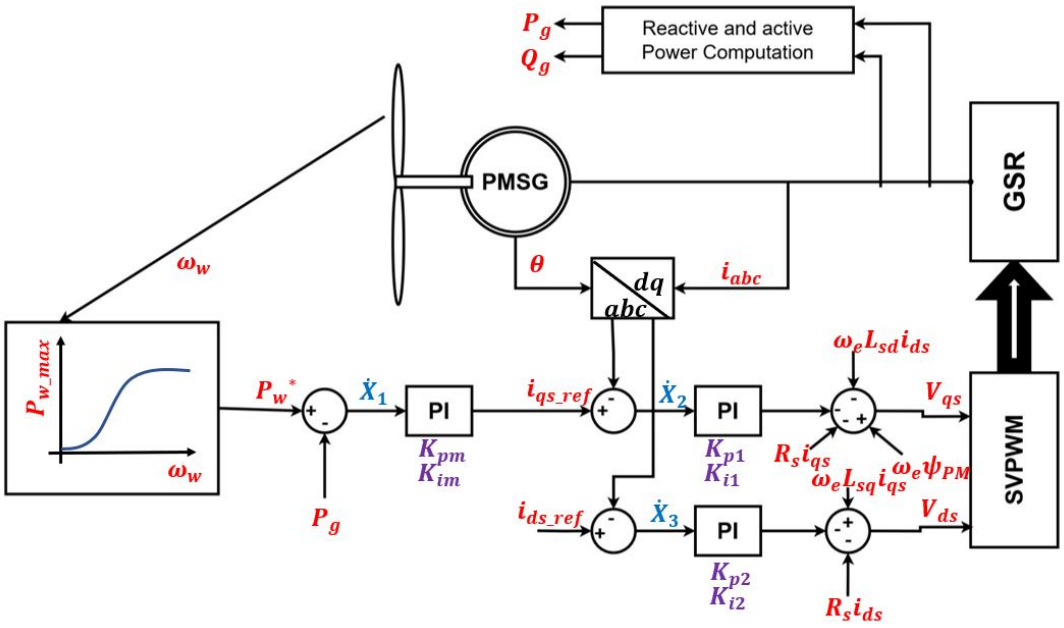

Fig. 2.7. *Generator side Converter*

$$i_{ds_{ref}} = 0 \tag{2.39}$$

$$\dot{X}_1 = P_{W_{ref}} - P_G \tag{2.40}$$

$$\dot{X}_2 = i_{qs_{ref}} - i_{qs} \tag{2.41}$$

$$\dot{X}_3 = i_{ds_{ref}} - i_{ds} \tag{2.42}$$

where

$$i_{qs_{ref}} = K_{pm}\dot{X}_1 - K_{im}X_1$$

$$V_{ds} = \omega_e L_{sq} i_{qs} - R_s i_{ds} - K_{p2}\dot{X}_3 - K_{i2}X_3$$

$$V_{qs} = \omega_e \psi_{PM} - \omega_e L_{sd} i_{ds} - R_s i_{qs} - K_{p1}\dot{X}_2 - K_{i1}X_2$$

In the given equations, i_{ds_ref} and i_{qs_ref} represent the reference currents on the direct and quadrature axes, respectively. P_{W_ref} and P_G indicate the reference power from the wind turbine and the actual generated power. The actual direct and quadrature axis currents are denoted by i_{ds} and i_{qs}, while X_1, X_2, and X_3 act as intermediate state variables in the control scheme. Controller gains are represented by K_{pm}, K_{im}, K_{p1}, K_{i1}, K_{p2}, and K_{i2}. Direct and quadrature axis voltages are symbolized by V_{ds} and V_{qs}. Other essential parameters include the self-inductances L_{sq} and L_{sd} on their respective axes, the stator resistance R_s, the electrical angular frequency ω_e, and the flux linkage due to permanent magnets, ψ_{PM}. The state equations are shown in equation (2.43).

$$\Delta \dot{X_{rsc}} = A_{rsc}\Delta X_{rsc} + B_{rsc}\Delta U_{rsc} \tag{2.43}$$

$$\Delta X_{rsc} = [\Delta X_1 \quad \Delta X_2 \quad \Delta X_3]^T$$

$$\Delta U_{rsc} = [\Delta V_{ds} \quad \Delta V_{qs} \quad \Delta i_{ds} \quad \Delta i_{qs} \quad \Delta P_{wref} \quad \Delta \omega_2]^T$$

2.1.2.5 DC Link Model

DC link performs multiple functions. It acts as a short-term energy storage or buffer, smoothing out the intermittently generated power from wind. Additionally, it facilitates voltage conversion, converting the variable voltage output from the generator-side rectifier into a stable DC voltage, which is then inverted to produce grid-compatible AC power. DC link supports power electronic conversion while filtering out harmonics and high-frequency noise and ensuring high power quality delivery to the grid. DC link primarily consists of a capacitor and the dynamics are mainly governed by that capacitor. The used DC link model in this study is shown in figure 2.8 . The power loss in the

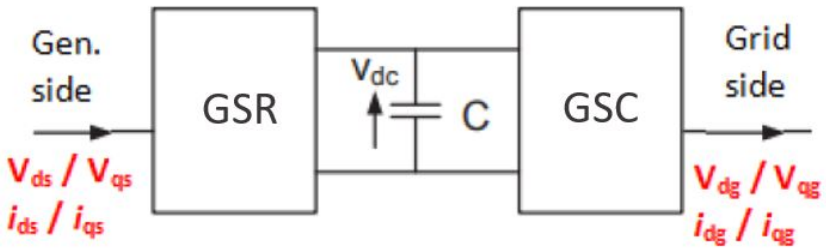

Fig. 2.8. *DC link model*

converter is small compared to the power transfer through the converter. Therefore assuming no active power loss in the converters,

$$\text{Capacitor Power} = \text{Generator Power} - \text{Delivered Power}$$

$$0.5CV_{dc}^2 = (V_{ds}i_{ds} + V_{qs}i_{qs}) - (V_{dg}i_{dg} + V_{qg}i_{qg}) \tag{2.44}$$

The linearized equations are given in (2.45)

$$\Delta\dot{X}_{dc} = A_{dc}\Delta X_{dc} + B_{dc}\Delta U_{dc} \tag{2.45}$$

$$\Delta X_{dc} = \Delta V_{dc}$$

$$\Delta U_{dc} = [\Delta V_{dg} \quad \Delta V_{qg} \quad \Delta i_{dg} \quad \Delta i_{qg} \quad \Delta V_{ds} \quad \Delta V_{qs} \quad \Delta i_{ds} \quad \Delta i_{qs}]^T$$

2.1.2.6 Grid Side Converter Model

The primary function of the GSC is to facilitate the wind turbine system with the electrical grid. It converts DC power to AC, ensuring it matches the frequency, voltage and phase of the grid. GSC is pivotal in maintaining power quality, ensuring minimal harmonic distortions, and providing advanced grid support capabilities such as voltage regulation, reactive power compensation, and fault ride-through. In essence, the GSC ensures that the harvested wind energy is seamlessly integrated and synchronized with the existing grid infrastructure. The Fig. 2.9 shows the control schematic of the GSC. The dynamic equations are in equations (2.46) to (2.49)(12).

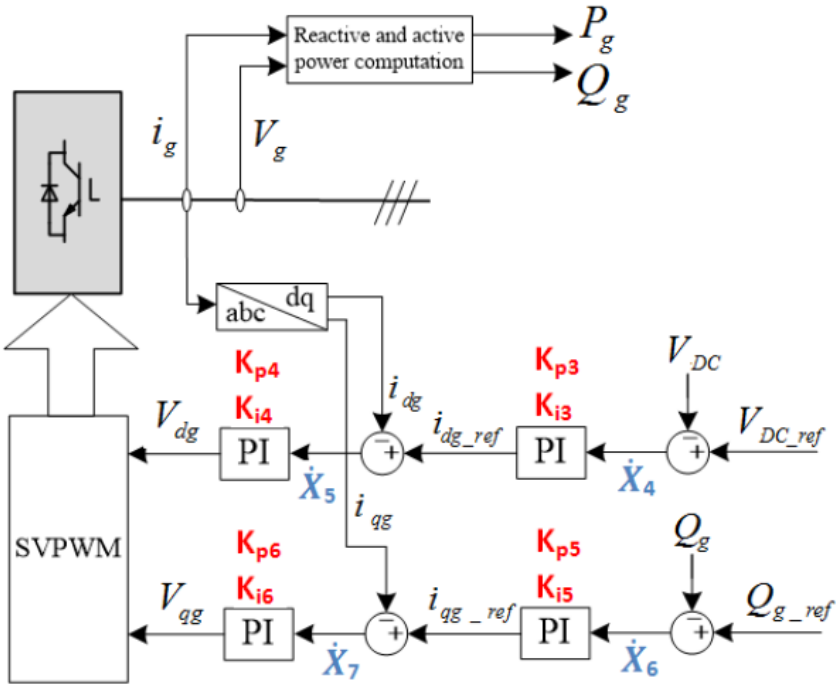

Fig. 2.9. *Grid side converter model*

$$\dot{X}_4 = V_{DC_{ref}} - V_{DC} \tag{2.46}$$

$$\dot{X}_5 = i_{dg_{ref}} - i_{dg} \tag{2.47}$$

$$\dot{X}_6 = Q_{g_{ref}} - Q_g \tag{2.48}$$

$$\dot{X}_7 = i_{qg_{ref}} - i_{qg} \tag{2.49}$$

$$i_{dg_{ref}} = K_{p3}\dot{X}_4 + K_{i3}X_4$$

$$V_{dg} = K_{p4*}\dot{X}_5 + K_{i4}X_5$$

$$i_{qg_{ref}} = K_{p5}\dot{X}_6 + K_{i5}X_6$$

$$V_{qg} = K_{p6}\dot{X}_7 + K_{i6}X_7$$

In the provided set of equations, the terms $\dot{X}_i$ represent the rates of change of various state variables in the wind power plant system. The quantities $V_{DC_{ref}}$ and V_{DC} correspond to the reference and actual DC voltage values, respectively. The variables $i_{dg_{ref}}, i_{qg_{ref}}$ denote the reference d-axis and q-axis currents, while i_{dg} and i_{qg} indicate the actual currents in these axes for the GSC. $Q_{g_{ref}}$ stands for the reference reactive power, and Q_g signifies the actual reactive power supplied to the grid. The controller gains are represented by terms with K_p and K_i, which are utilized in control strategies to fine-tune the power output and ensure optimal system performance. The linearized equation is given in equation (2.62)

$$\Delta\dot{X_{gsc}} = A_{gsc}\Delta X_{gsc} + B_{gr}\Delta U_{gsc} \tag{2.50}$$

$$\Delta X_{gsc} = [\Delta X_4 \quad \Delta X_5 \quad \Delta X_6 \quad \Delta X_7]^T$$

$$\Delta U_{gsc} = [\Delta V_{dcref} \quad \Delta Q_{gref} \quad \Delta V_{dc} \quad \Delta i_{qg} \quad \Delta i_{dg} \quad \Delta i_{qg}]^T$$

2.1.3 Solar Power Plants

The solar power plant model is shown in figure 2.10, When modeling a solar power plant, especially for control and dynamic analyses, simplifying assumptions are often made to reduce the complexity of the mathematical model without compromising its accuracy for the purpose at hand. When modeling a solar power plant, especially for control and dynamic analyses, the following simplifying assumptions are often made:

1. **Neglecting the Effect of the Output Filter Capacitor C_f:**
   The output filter capacitor in VSC is primarily for high-frequency filtering. Since the focus is on the low-frequency band, the high-frequency filtering effects of C_f can be neglected. This simplifies the model by not considering the dynamics and resonances associated with the filter capacitor.

2. **Assuming Lossless System with Specified Resistances:**

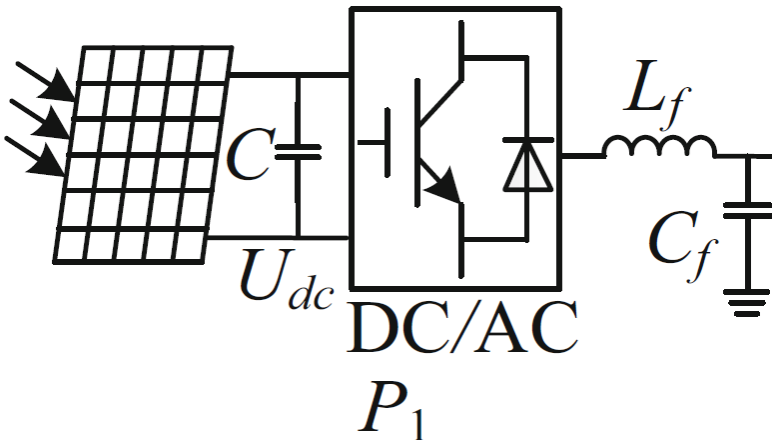

Fig. 2.10. *Configuration of PV generation*

All components, like converters, lines, and transformers, are ideal and do not introduce any losses, except for the specific resistances explicitly included in the model.

These assumptions help simplify the mathematical model and the control design for a solar power plant.

2.1.3.1 PV Array Model

The configuration of the photovoltaic (PV) array is depicted in figure 2.11. Here, N_p and N_s denote the number of cells connected in parallel and series, respectively. The DC current is symbolized by I_{PV}. The current-voltage (U-I) relationship of a PV cell, provided by manufacturers, is described by(7):

$$I_o = I_{sc}\left(1 - C_1 e^{\frac{U_{dc}}{h - C_2 U_{oc}}} - 1\right) \tag{2.51}$$

In this equation, I_{sc} represents the short-circuit current, and U_{oc} is the open-circuit voltage. The coefficients C_1 and C_2 can be computed using:

$$C_1 = \left(1 - \frac{I_m}{I_{sc}}\right) e^{-\frac{U_m}{C_2 U_{oc}}} \tag{2.52}$$

$$C_2 = \frac{U_m}{U_{oc}} - 1 \ln\left(1 - \frac{I_m}{I_{sc}}\right) \tag{2.53}$$

Where I_m and U_m stand for the current and voltage at the maximum power point, respectively. These values are generally supplied by the PV array manufacturer. Furthermore, they can be adjusted, as outlined in Equation (5), to account for changes in external conditions. In PV systems, the performance and characteristics of the solar panels are paramount. The current I_{sc} under short-circuit conditions is related to

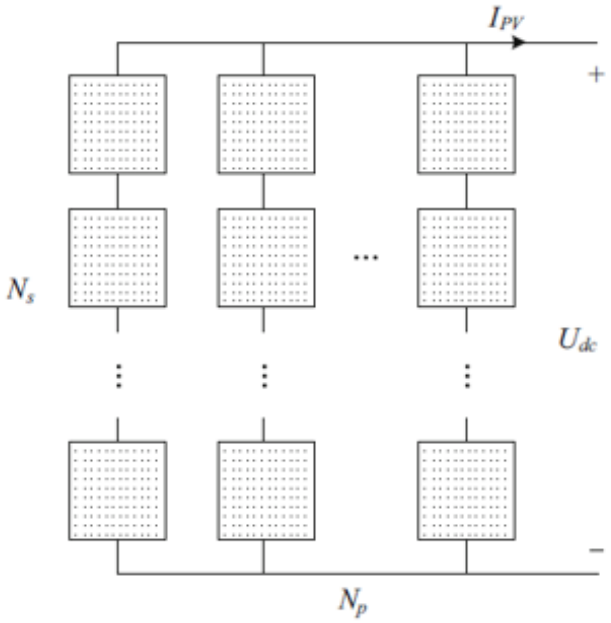

Fig. 2.11. *Configuration of PV arrayl*

a reference value $I_{sc;\text{ref}}$ and is influenced by the ratio of the actual output power S to a reference power S_{ref}, as well as any change in temperature (ΔT) from standard conditions(7). This relationship is expressed as:

$$I_{sc} = \frac{I_{sc;\text{ref}} \times S}{S_{\text{ref}}}(1 + a\Delta T)$$

Similarly, the open-circuit voltage U_{oc} is given by:

$$U_{oc} = U_{oc;\text{ref}} \ln(e + b\Delta S)(1 - c\Delta T)$$

Where DS signifies the difference in solar irradiance from reference conditions. The current I_m at the MPP and the voltage U_m at MPP can be described respectively as:

$$I_m = \frac{I_{mc;\text{ref}} \times S}{S_{\text{ref}}}(1 + a\Delta T)$$

$$U_m = U_{mc;\text{ref}} \ln(e + b\Delta S)(1 - c\Delta T)$$

It's important to note that the subscripts "ref" stand for reference values typically provided under standard test conditions. The variables a, b, and c are specific parameters derived from the manufacturer's data sheets. Expanding on the I-U characteristics for the PV array, the relationship between the DC voltage U_{dc} and the array's output cur-

rent I_{PV} can be formulated taking into account the dimensions of the array:

$$I_{PV} = N_p I_{sc} \left[1 - C_1 \left(e^{\frac{U_{dc}}{C_2 N_s U_{OC}}} - 1 \right) \right]$$

Where N_p represents the number of cells connected in parallel and N_s denotes the cells in series.

2.1.3.2 VSC Control Strategy Model

In Fig. 2.12, we present a vector control system designed for a VSC which is primarily influenced by grid voltage. The PV array delivers both the DC voltage, labeled U_{dc}, and the DC current, designated I_{PV}. The Maximum Power Point Tracking (MPPT) controller interprets these inputs and subsequently produces the desired reference DC voltage, $U_{dc,\text{ref}}$. Within the d-frame, the exterior control layer focuses on this DC voltage, directing the formation of its associated reference current, $i_{d,\text{ref}}$. In tandem, the q-frame's outer loop monitors the AC-bus voltage, leading to the conception of its reference current, $i_{q,\text{ref}}$. The inner controllers craft modulation signals within the dq domain, which are adeptly reverted to the abc realm. Moreover, the Phase-Locked Loop (PLL) manifests an output phase, captured as Θ_{pll}. As per the controller dy-

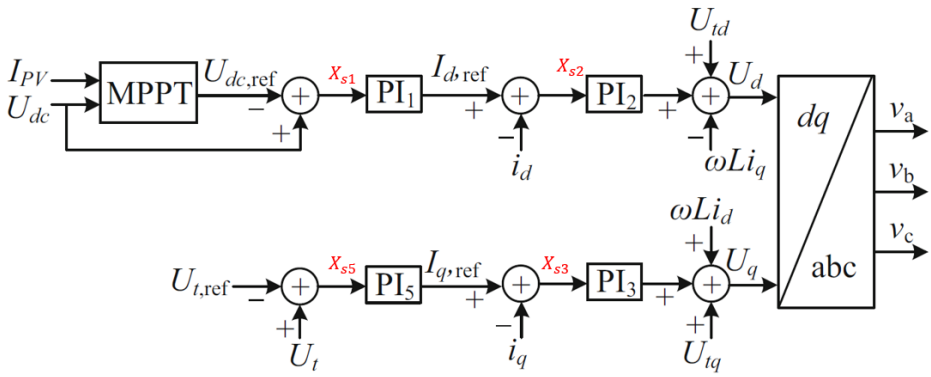

Fig. 2.12. *Control strategy of VSC*

namic equations can be obtained as shown in (2.54) to (2.59) :

$$\frac{dX_{s1}}{dt} = U_{dc} - U_{dc,\text{ref}} \tag{2.54}$$

$$\frac{dX_{s2}}{dt} = k_{p1}(U_{dc} - U_{dc,\text{ref}}) + k_{i1}X_{s1} - i_d \tag{2.55}$$

$$\frac{dX_{s5}}{dt} = U_t - U_{t,\text{ref}} \tag{2.56}$$

$$\frac{dX_{s3}}{dt} = k_{p5}(U_t - U_{t,\text{ref}}) + k_{i5}X_{s5} - i_q \tag{2.57}$$

$$U_d = k_{p2}[k_{p1}(U_{dc} - U_{dc,\text{ref}}) + k_{i1}X_{s1} - i_d] + k_{i2}X_{s2} + U_{td} - \omega L i_q \tag{2.58}$$

$$U_q = k_{p3}[k_{p5}(U_t - U_{t,\text{ref}}) + k_{i5}X_{s5} - i_q] + k_{i3}X_{s3} + U_{tq} + \omega L i_d \tag{2.59}$$

In the equations the Variables U_{dc} and $U_{dc,\text{ref}}$ signify the actual and the reference DC voltages, respectively. The coefficients k_{p1}, k_{i1}, k_{p2}, k_{i2}, k_{p3}, k_{i3}, k_{p5}, and k_{i5} stand as the proportional and integral gains of various controllers, determining the system's responsiveness to discrepancies. Current components i_d and i_q symbolize the orthogonal components, common in vector control systems. U_t depicts the terminal voltage, while $U_{t,\text{ref}}$ is its reference. The direct and quadrature breakdowns of this voltage are represented as U_{td} and U_{tq}. The control strategy of the PLL is shown in figure 2.13 and the dynamic equations are as shown in equation (2.60) and equation (2.61).

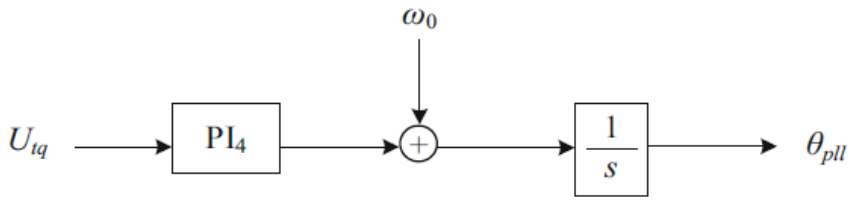

Fig. 2.13. *Control strategy of PLL*

$$\frac{dx_{\text{pll}}}{dt} = U_{tq} \tag{2.60}$$

$$\frac{d\Theta_{\text{pll}}}{dt} = k_{p4}U_{tq} + k_{i4}x_{\text{pll}} + \omega_0 \tag{2.61}$$

In here k_{p4} and k_{i4} are the parameters of PLL. By linearizing around the above all equations can be expressed as follows.

$$\Delta\dot{X}_{slr} = A_{slr}\Delta X_{slr} + B_{slr}\Delta U_{slr} \tag{2.62}$$

and

$$\Delta X_{slr} = \begin{bmatrix} \Delta X_{s1} & \Delta X_{s2} & \Delta X_{s3} & \Delta X_{s5} & \Delta X_{pll} & \Delta\theta_{pll} & \Delta U_{dc} \end{bmatrix}^T$$

$$\Delta U_{slr} = \begin{bmatrix} \Delta U_{dc,ref} & \Delta U_t & \Delta U_{tq} & \Delta i_d & \Delta i_q & \Delta i_{PV} & \Delta U_{td} \end{bmatrix}^T$$

2.2 Network Moedling

In power system studies, network modeling plays a crucial role, and it provides a foundation for understanding and analyzing the interactions between the network and other interconnected components including generators, transformers, transmission lines, loads, etc. Accurate modeling of the network is the key to predict system behavior under var-

ious conditions (load fluctuations, integration of renewable energy sources, varying transmission capacities, disturbances due to faults or equipment failures, and dynamic demand scenarios). Depending on the focus of the study and the computational ability different types of network representations are available. The constant admittance representation offers a simplified view of the network and is suitable for steady-state studies. The Detailed representation provides a comprehensive model of the power network including their most detailed form and this method is computationally intensive due to this high degree of detail. However, the complexity and the high computational power requirements is the disadvantage of detail representation. The dynamic phasor network modeling captures both the steady state and dynamic behavior of the system and this method is computationally intensive for tracking fast transients and high-frequency dynamics. This method is not as accurate as the detailed representation but it is accurate enough to do this small signal stability analysis(3)(13).

2.2.1 Constant Admittance Matrix Representation

When the network is modeled using the power frequency admittance matrix in electromechanical oscillation studies, the AC network dynamics are ignored. This matrix captures the relationships between various nodes within the power system. Specifically, it describes how changes in node voltages relate to the injections of current at those nodes. This simplified representation allows for the analysis of electromechanical oscillations, which are crucial for studying the stability and behavior of the power system under various operating conditions and disturbances. The relationship between node voltage and the node current injections is given by the equation (2.63) (3).

$$\left[\Delta I\right] = \left[Y_{\text{bus}}\right] \left[\Delta V\right] \tag{2.63}$$

In this equation, ΔI represents the change in currents injected by the dynamic devices at the busbars,ΔV represents the change in voltage of those bus bars and Y_{bus} is the bus admittance matrix and it is calculated using the power frequency admittance of the network components.

2.2.2 Dynamic Phasor Network Model

In this method transmission line components in the power system are represented by using differential equations. Here, the transmission lines are modeled using series resister-inductor (RL) components and parallel resistor-capacitor (RC) components. These equations are initially formulated in the time domain via Kirchhoff's laws and they are transferred to the phasor domain through Laplace or Fourier transformation. The base of this method is briefly described below.
The time domain representation of an AC current using complex exponentials can be

expressed as in the equation (2.64) (13).

$$i_{ac} = A_m e^{j\phi} e^{j\omega_0 t} = A_m[\cos(\phi) + j\sin(\phi)]e^{j\omega_0 t} \tag{2.64}$$

Where the A_m is the magnitude of the current and the ϕ is the phase while the ω_0 is the system frequency. The equation (2.64) can be expressed in terms of rectangular coordinate components of the phasor components as shown in the equation (2.65). Here the oscillatory frequencies generated by the dynamic devices are included in the phasor current.

$$i_{ac}(t) = (I_R + jI_I)e^{j\omega_0 t} \tag{2.65}$$

$$I_R = A_m cos(phi)$$

$$I_I = A_m sin(phi)$$

As described above in this method most of the AC network components are represented as series RL components and parallel RC components. The linearized model development for those RL and RC components is described below.

2.2.2.1 Series RL Components

Consider a series RL circuit connected between nodes 1 and 2. The instantaneous voltage across nodes 1 and 2 can be written as shown in equation (2.66) and the complex rotating phasor relationships of the currents and voltages are substituted into equation (2.67)(13).

$$V_{12} = L\frac{di_{12}}{dt} + Ri_{12} \tag{2.66}$$

$$(V_R + jV_I)e^{j\omega_0 t} = L\frac{d(I_R + jI_I)e^{j\omega_0 t}}{dt} + R(I_R + jI_I)j\omega_0 e^{j\omega_0 t} \tag{2.67}$$

By considering the nominal frequency ω_0 is constant the equation (2.68) is obtained.

$$V_R + jV_I = L\frac{d(I_R + jI_I)}{dt} + (R + j\omega_0 L)(I_R + jI_I) \tag{2.68}$$

$$V_R = (V_{1R} - V_{2R})$$

$$V_I = (V_{1I} - V_{1I})$$

here V_{1R},V_{1I}, V_{2R}, and V_{2I} are the real and imaginary parts of the phasor voltage difference between nodes 1 and 2. The equation (2.69) is obtained by linearizing the

equation (2.68). All the values in per unit so ω_0/L term appear instead of $1/L$ term.

$$\begin{bmatrix} \dot{I}_R \\ \dot{I}_I \end{bmatrix} = \begin{bmatrix} \frac{-R\omega_0}{L} & \omega_0 \\ -\omega_0 & \frac{-R\omega_0}{L} \end{bmatrix} \begin{bmatrix} \Delta I_R \\ \Delta I_I \end{bmatrix} + \begin{bmatrix} \frac{\omega_0}{L} & 0 & \frac{-\omega_0}{L} & 0 \\ 0 & \frac{\omega_0}{L} & 0 & \frac{-\omega_0}{L} \end{bmatrix} \begin{bmatrix} \Delta V_{1R} \\ \Delta V_{1I} \\ \Delta V_{2R} \\ \Delta V_{2I} \end{bmatrix} \tag{2.69}$$

2.2.2.2 Parallel RL Component

Consider a parallel RC circuit connected between node 1 and the ground. The instantaneous current injected to the circuit can be written as shown in equation xx

$$i = C\frac{dv_1}{dt} + \frac{1}{R}v_1 \tag{2.70}$$

the phasor relationship similar to equation (2.68) given by,

$$I_R + jI_I = C\frac{d(V_{1R} + jV_{1I})}{dt} + (\frac{1}{R} + j\omega_0 C)(V_{1R} + jV_{1I}) \tag{2.71}$$

By linearizing the above equation is shown by equation (2.72) and as in the previous case all the values are in pu and ω_0/C term appears instead of $1/c$.

$$\begin{bmatrix} \dot{V}_{1R} \\ \dot{V}_1 I \end{bmatrix} = \begin{bmatrix} \frac{-\omega_0}{RC} & \omega_0 \\ -\omega_0 & \frac{-\omega_0}{RC} \end{bmatrix} \begin{bmatrix} \Delta V_{1R} \\ \Delta V_{1I} \end{bmatrix} + \begin{bmatrix} \frac{\omega_0}{C} & 0 \\ 0 & \frac{-\omega_0}{C} \end{bmatrix} \begin{bmatrix} \Delta I_R \\ \Delta I_I \end{bmatrix} \tag{2.72}$$

The same methodology is used to model all the R-L-C components within the AC network. The comprehensive network model, which encompasses state variables such as inductor currents and capacitor voltages, is derived by applying Kirchhoff's law to combine these currents and voltages.

2.2.2.3 The Network Models Used In This Research

Figure 2.14 shows the used power system in this research, and it is a simplified representation of a power network designed to capture essential features and phenomena observed in real-world systems and it offers a unique configuration that makes it suitable for this power system study. This system contains 12 buses with 4 power sources as shown in the bellow figure (14). All the data including bus data (voltage level, type, load data, etc.), generator data, and transmission line data (resistance, reactance, susceptance, etc.) are shown in Appendix 1.
The network models related to the case study (up to 220kV and upto 132kV) of Sri Lankan power system is presented under 3.6 and 3.7

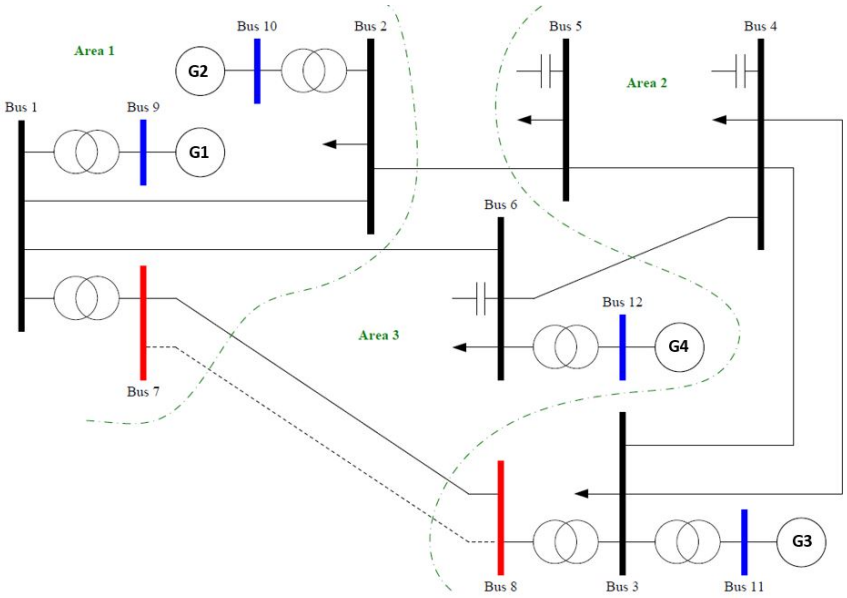

Fig. 2.14. *Single line diagram of the 12-bus test system*

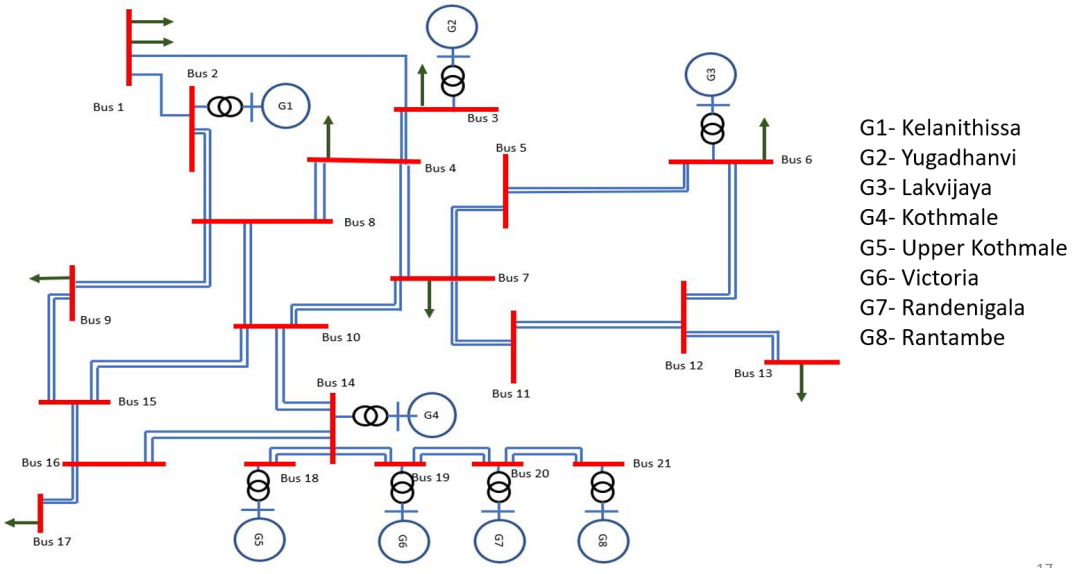

Fig. 2.15. *Single line diagram of the Sri Lankan power System up to 220kV*

2.3 Common Reference Frame

To ensure a unified understanding of the dynamic behavior across various components, it is crucial to express all these behaviors in a singular reference frame. As discussed in the previous sections, each component inherently operates within its unique d-q reference frame, pivoting at the pace of its rotor's rotation as shown in figure 2.17. In undertaking a comprehensive small signal stability analysis, it's essential to utilize a common reference frame rotating at synchronous speed. This unifying frame, known as the R-I frame, seamlessly integrates the dynamics of all devices within the broader

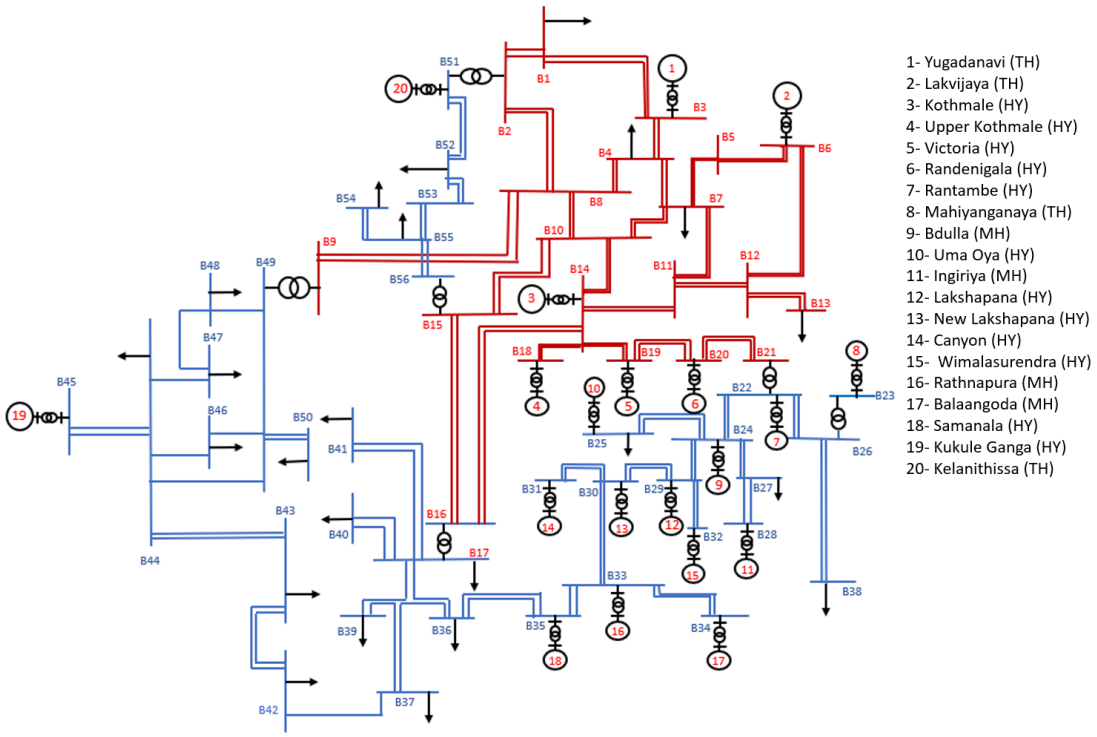

Fig. 2.16. *Single line diagram of the Sri Lankan power System up to 132kV*

network context (13).

The translation of voltages and currents from the d-q domain to this common R-I frame is achieved through the transformation equations presented in (2.73) and (2.74). These equations essentially leverage trigonometric relationships, given the periodic nature of AC signals. It's essential to note that for the sake of accuracy in subsequent analyses, these transformation equations must be linearized around the established operating point.

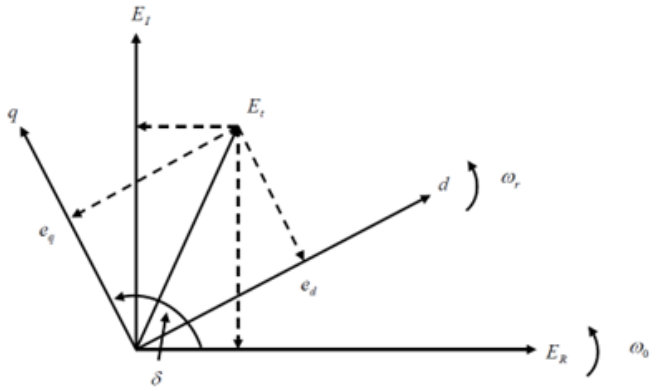

Fig. 2.17. *Transformation from individual machine d-q frame to common reference*

$$\begin{bmatrix} e_q \\ e_d \end{bmatrix} = \begin{bmatrix} \cos\delta & \sin\delta \\ sin\delta & -\cos\delta \end{bmatrix} \begin{bmatrix} E_R \\ E_I \end{bmatrix} \tag{2.73}$$

$$\begin{bmatrix} i_q \\ i_d \end{bmatrix} = \begin{bmatrix} \cos\delta & \sin\delta \\ sin\delta & -\cos\delta \end{bmatrix} \begin{bmatrix} I_R \\ I_I \end{bmatrix} \tag{2.74}$$

By adopting to this common reference frame makes it easier to analyze and understand the power system's dynamic behavior in a unified way.

2.4 Aggregate Small Signal Model Development

Following the establishment of the common reference frame in the previous section, the linearized equations for each component can now be seamlessly combined to derive a unified linearized state-space model for the entire power system. This representation effectively captures the collective dynamics of the system, as clearly illustrated by the below equations:

$$\Delta\dot{X} = A\Delta X + B\Delta U \tag{2.75}$$

$$\Delta\dot{Y} = C\Delta X + D\Delta U \tag{2.76}$$

These equations effectively detail the relationships within the power system, offering an analytical method that links individual component behaviors to the overall system dynamics.

2.5 The Test Scenarios

Within this research, attention is drawn to five carefully constructed scenarios shown in bellow. Each is designed to offer insights into the intricacies of power system behavior under different configurations.

1. **Scenario 1: All conventional sources with the constant admittance network representation**
   In this scenario, four generators connected to bus 9,10,11,12 were considered as synchronous generators with their auxiliary controllers as described in the above sections, and the network is modeled in constant adm, instance network modeling method. The linearized equations of all four generators and the network equations can be combined to form the overall state space equation in the form of (2.75). In this case, there are 56 state variables including 14 states from each conventional power plant but not any from the network. This scenario examines the stability of the power system comprising solely conventional sources and it

provides a baseline for comparison against the two-network modeling method which is used in this research.

2. **Scenario 2: All conventional sources with the dynamic network representation**
   In this scenario, the previous setup is enhanced by integrating the inherent dynamics associated with transmission lines and various network elements. By contrasting this configuration with the first scenario, the impact of these network dynamics on small signal stability can be discerned. In this case, there are 108 state variables including 16 states from each conventional power plant and 44 states from the network. This scenario serves as a comparative reference, enabling the contrast of the effects of dynamic network representation with the more static constant admittance approach explored in the first scenario.

3. **Scenario 3: Conventional + non-conventional source (wind plant) with the dynamic network representation**
   In this scenario, the integration of a non-conventional power source, specifically a type 4 wind power plant, is taken into consideration. The traditional power plant previously connected to bus number 12 is substituted with this wind power plant. The primary objective here is to gauge the influence such an integration has on the stability of the overall power system. In this case, there are 106 state variables including 16 states from each 3 conventional power plants, 14 state variables from the wind power plant, and 44 states from the network. Various levels of wind power penetration, including 17%, 25%, and 30%, are considered to evaluate the effects of different levels of renewable power on system stability.

4. **Scenario 4: Conventional + non-conventional source (solar plant) with the dynamic network representation**
   In Scenario 4, paralleling the approach in Scenario 3, the focus shifts to the incorporation of solar energy into the system. The traditional power plant connected to bus no 12 is supplanted by a solar power facility. This examination offers insights into the combined impacts of both conventional and solar energy on the system's small signal stability. In this case, there are 99 state variables including 16 states from each of 3 conventional power plants, 7 state variables from solar power plants, and 44 states from the network. Penetration levels of solar power, specifically at 17%, 25%, and 30%, are assessed to provide a holistic understanding of varying renewable energy contributions to the system's overall stability.

5. **Scenario 5: Conventional + non-conventional sources (solar plant + wind plant) with the dynamic network representation**
   The final scenario investigates the simultaneous integration of both wind and

solar power plants into the power system. In this scenario, conventional power plants which are connected to bus no 12 and bus 11 are replaced by wind and solar power plants respectively. This allows us to investigate the combined effect of solar, wind, and conventional power plants on the system's small signal stability. In this case, there are 97 state variables including 16 states from each generator 2 conventional power plants, 14 states from wind plant, 7 states from the solar power plant, and 44 states from the network. Here both wind and solar penetration levels are 25% each.

Apart from the above-described five scenarios, a key aspect of this research will focus on the Sri Lankan power system as a case study. under this caase study four scenarios are available as shows in bellow.

1. **Scenario 1A : Sri Lankan network up to 220 kV level**
   In this scenario of the Sri Lankan power system case study, the 220kV level of the Sri Lankan power system is examined. This system contains 21 buses, with 8 power plants of which five hydro sources, and three thermal sources. To achieve an accurate representation of the network, the Dynamic Phasor Model has been employed. This methodical approach provides insights into 219 state variables, allowing for a thorough analysis.

2. **Scenario 2A: Sri Lankan network up to 220 kV level with Mannar Wind power plant**
   In this scenario of the Sri Lankan power system case study, In here the Mannar wind power plant is connected to the system. It is connected to the 13^{th} bus of the system. This wind plant is modeled as an aggregate model to reduce the complexity of the study. In addition to the 8 power plants in the previous scenario (which include five hydro sources and three thermal sources), this scenario introduces the additional wind power plant to the system. Consistent with the approach in the first scenario, the network is represented using the Dynamic Phasor Model. This system contains 233 state variables.

3. **Scenario 3A : Sri Lankan network up to 132 kV level**
   In this scenario of the Sri Lankan power system case study, the 132kV level of the Sri Lankan power system is examined. This system contains 56 buses, with 20 power plants of which 16 hydro sources, and 4 thermal sources. To achieve an accurate representation of the network, the Dynamic Phasor Model has been employed. This system contains 571 state variables.

4. **Scenario 4A: Sri Lankan network up to 132 kV level with Mannar Wind power plant**
   In the given scenario of the Sri Lankan power system case study, the Mannar

wind power plant has been integrated. It's connected to the 13th bus within the system. To reduce complexity, the wind plant has been represented as an aggregate model (same model used in scenario 2A). Alongside the 20 power plants from the previous scenario, including 16 hydro and 4 thermal sources, this model introduces an additional wind power plant. As in the initial scenario, the Dynamic Phasor Model is employed to represent the network. This configuration encompasses 585 state variables.

2.6 Chapter Summery

This chapter focuses on the mathematical models of power system components that are used in this small signal study. It starts by discussing the modeling techniques for power plants, including conventional sources and the auxiliary controllers, wind power plants, and solar power plants. The chapter then transitions into network modeling, introducing the constant admittance matrix representation and the dynamic phasor network representation. This chapter describes the modeling of the small signal model by using the common reference frame technique. Then it describes the network models that are used in each scenario under this research and briefly describes all the test scenarios and the real-world case study scenarios.

CHAPTER 3

RESULTS AND ANALYSIS

In the following chapter, the results and analysis derived from the conducted research are presented. Initially, attention is placed on model validation, ensuring that the methodologies and representations used are anchored in reliability and precision. Subsequently, insights from each of the scenarios examined are presented. Through a detailed comparison and analysis of these outcomes, a comprehensive understanding of the system's behavior under different conditions is offered, highlighting the intricate factors influencing power system dynamics.

3.1 Model Validation

In the domain of power system analysis, ensuring the validity of a chosen model stands as a essential requirement. The approach taken within this research was no exception. The dynamic equations, foundational to the methodology, were subjected to linearization around a designated operating point, a step indispensable for facilitating small signal stability analysis. It is very important to ascertain that this linear representation accurately mirrors the system dynamics.

In addressing this crucial aspect, a proven and time-tested approach was adopted. The linear system's responses were methodically compared to those of its nonlinear counterpart, with both systems subjected to identical, predefined, small disturbances. From the vast array of simulation tools available for power system studies, EMT-type simulations conducted via the PSCAD software were chosen for this research due to their established accuracy in the field.

Expanding upon the constructed scenarios, from the initial to the final, the focus was placed on the speed variation of the synchronous generator connected to bus 9. Intentionally, disturbances in the form of step changes, ranging between 0.2% and 0.6%, were introduced into the governor speed reference of this generator. While these disturbances were of a minor scale, they were crucial in testing the accuracy of the model's representation.

Upon analysis, it was observed that the responses obtained from the linear model simulations resonated closely with those derived from the nonlinear simulations. Such alignment in outcomes is not a mere coincidence but an affirmation of the model's reliability. The compatibility between linear and nonlinear simulations thus provides a foundational layer of confidence, solidifying the belief that the linearized models developed are not only sufficient but indeed optimal for forthcoming analyses.

In Figure 3.1, validation for Scenario 1 is depicted, wherein the generator connected to Bus 9 experiences a disturbance of a 0.6% step change in governor speed reference.

Similarly, Figure 3.2 showcases validation results for Scenario 2 with an identical disturbance of 0.6% step change in the governor speed reference of the generator at Bus 9. Moving on to Figure 3.3, the validation for Scenario 3 is illustrated, highlighting a 0.2% step change disturbance on the same generator. Figure 3.4 displays the validation results for Scenario 4, where the governor speed reference of the generator linked to Bus 9 undergoes a 0.4% step change disturbance. Finally, Figure 3.5 presents the validation for Scenario 5, emphasizing a 0.4% step change in the governor speed reference for the generator at Bus 9.

In examining the results, it's important to note some key details. For instance, in Scenario 1, while the output responses of PSCAD simulation show fluctuations, ut small signal model output response does not. This is because the small signal model of Scenario 1 neglects the stator dynamics of the synchronous generator and the network dynamics, unlike the detailed approach used in PSCAD. Similarly, minor differences between the PSCAD and small signal model output response graphs are observed in other scenarios as the small signal models typically simplify the system dynamics by linearizing around an operating point, neglecting certain nonlinearities and detailed system behaviors present in PSCAD simulations.

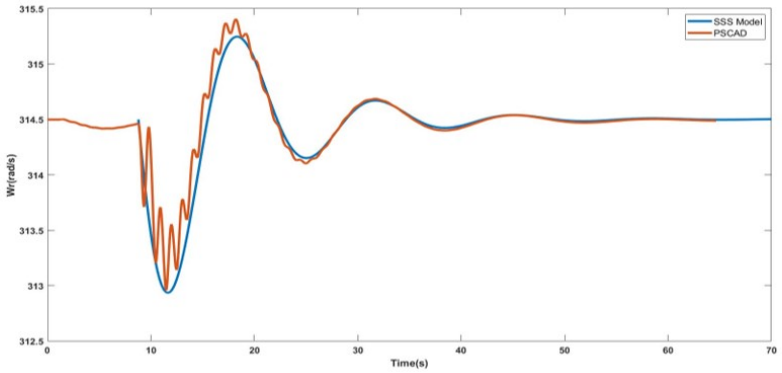

Fig. 3.1. *PSCAD and SS model Generator speed variation after small disturbance for scenario 1*

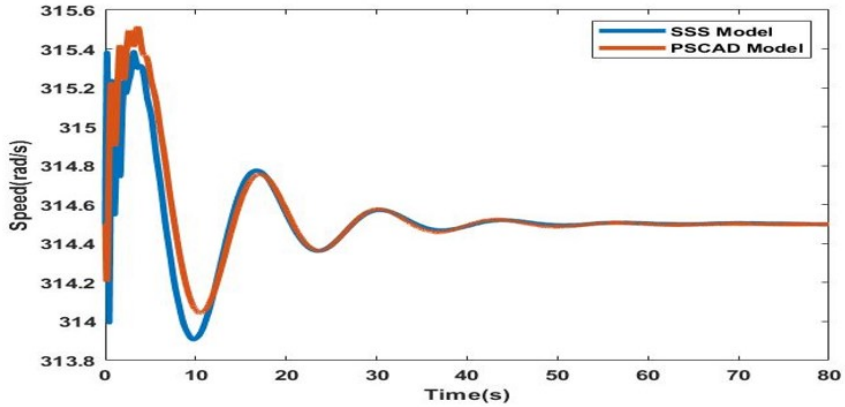

Fig. 3.2. *PSCAD and SS model Generator speed variation after small disturbance for scenario 2*

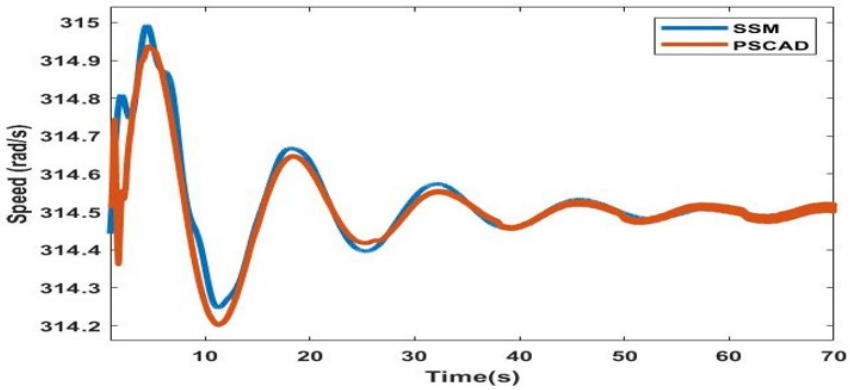

Fig. 3.3. *PSCAD and SS model Generator speed variation after small disturbance for scenario 3*

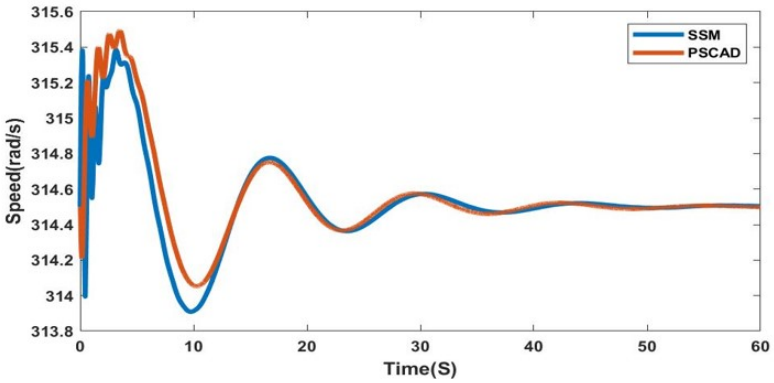

Fig. 3.4. *PSCAD and SS model Generator speed variation after small disturbance for scenario 4*

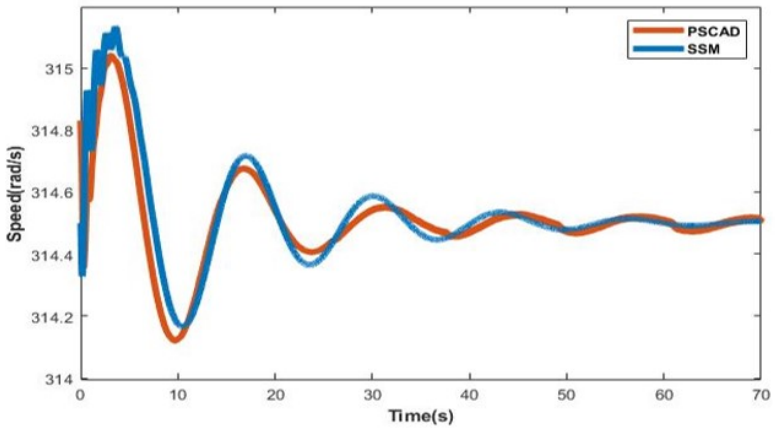

Fig. 3.5. *PSCAD and SS model Generator speed variation after small disturbance for scenario 5*

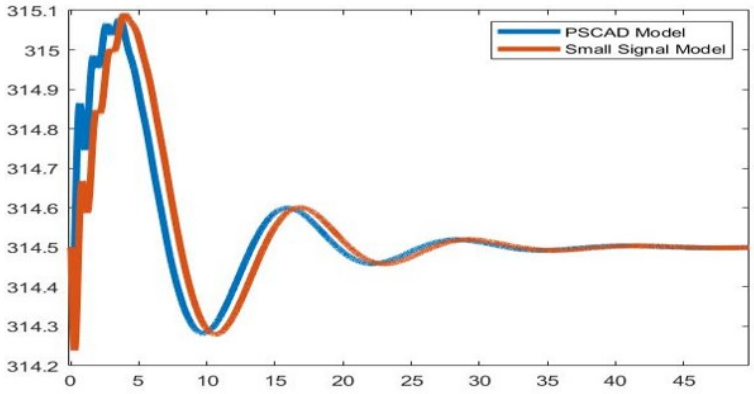

Fig. 3.6. *PSCAD and SS model Generator speed variation after small disturbance for scenario 1A*

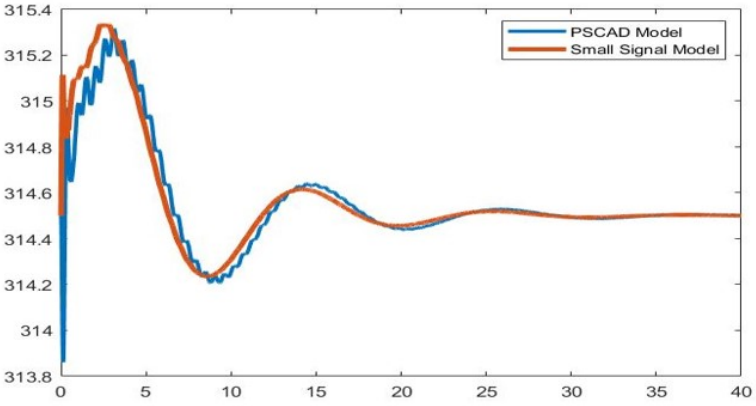

Fig. 3.7. *PSCAD and SS model Generator speed variation after small disturbance for scenario 2A*

3.2 Stability Analysis

This section focuses on the analysis of small signal stability in the power system by examining the eigenvalues, participation factors, oscillation frequency, and damping ratios to gain insights into the system's dynamic behavior and stability characteristics.

3.2.1 Scenario 1

In the thorough analysis conducted for Scenario 1, 56 eigenvalues associated with the state matrix of the given scenario were identified. Encouragingly, all of these eigenvalues were found to reside in the left half of the complex plane, signifying the stability of the system. Upon closer examination, 8 pairs of these eigenvalues were determined to be complex conjugates, indicating the existence of 8 oscillatory modes in the system. Further investigation revealed that, of these oscillatory modes, four—named A, B, C, and D for convenience—possessed damping ratios in the 13% to 14% range. In contrast, the other four were characterized by damping ratios exceeding 99.5%. To gain a deeper understanding of the influence of individual power plants on these oscillations, a comprehensive participation factor analysis was undertaken, with the results illustrated in figure 3.8. From this analysis, it was discerned that all four power plants were involved in the oscillations corresponding to mode A. For the subsequent modes, B was influenced by power plants 2 4, C by plants 1, 2, 3, and D by plants 1 3. Through this study, a deeper insight into the system's dynamics was obtained, highlighting the critical role of each power plant in the observed oscillatory behaviors.

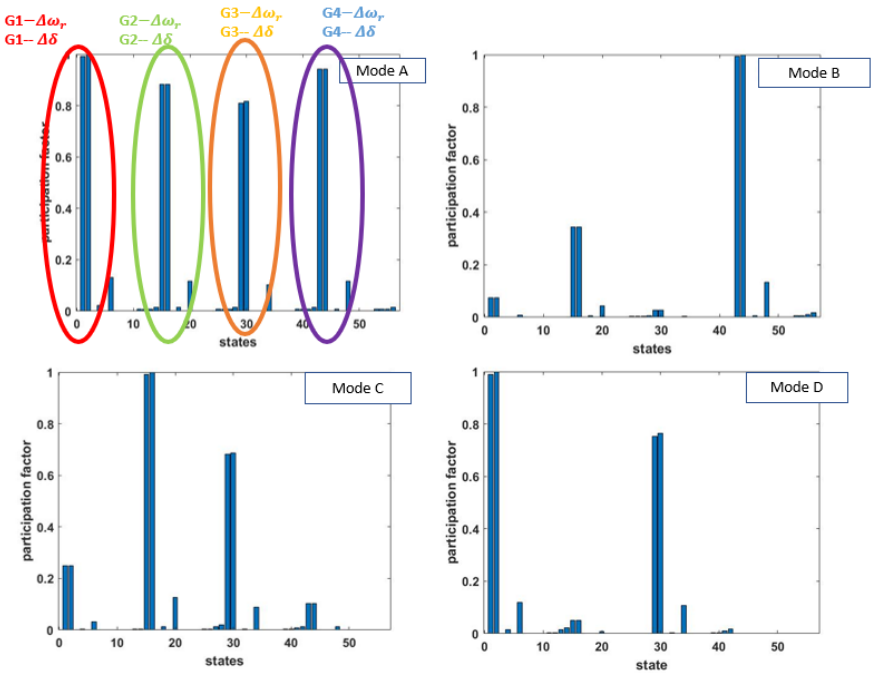

Fig. 3.8. *Participation Factors for modes with lower damping (scenario 1)*

3.2.2 Scenario 2

In transitioning to Scenario 2, a distinct differentiation emerges from Scenario 1, primarily in the employed network modeling technique. While Scenario 1 utilized the constant admittance matrix method, Scenario 2 adopted the dynamic phasor model approach. A total of 108 eigenvalues for the state matrix of scenario 2 were identified and eigenvalue examination confirmed the system's continued stability. However, a pronounced significant increase in the number of critical oscillatory modes was evident in Scenario 2 compared to its Scenario 1. Interestingly, among these modes, similar modes to those found in the previous scenario were identified and were subsequently labeled as A2, B2, C2, and D2. Interestingly these modes in Scenario 2 manifested marginally reduced damping ratios in contrast to those in Scenario 1. A meticulous participation factor analysis further unveiled the significant role of network dynamics in shaping these oscillatory modes as shown in the figure 3.9. This underscores the inherent influence of network interactions on the system's small signal stability attributes. By integrating these network dynamics, a holistic understanding of the system's dynamic response is achieved, thereby enhancing the precision of stability assessments. Moreover, beyond the modes identified and discussed from Scenario 1, Scenario 2 revealed several other modes with low damping ratios. Among these, five specific modes, named E2, F2, G2, H2, and I2, and they are the modes which the power plants significantly participated.

In the detailed analysis of Scenario 2, specific oscillatory behaviors were observed across distinct modes by using mode shape analysis as shown in figure 3.10. For Mode A2, all generators exhibited a coherent oscillation, moving mainly in the same direction, but they weren't perfectly in phase. The phase differences among them were narrow and limited to a range of just 10 degrees, underscoring a synchronized response across the generators with minor phase differences. Mode B2 unveiled another layer of system dynamics. Generators 1 and 2 oscillate coherently in one direction, contrasted by Generator 3, which moves in an opposing manner. This behavior highlights an interplay of forces within the system, with two generators harmonizing their movements while clashing with the third. In the case of Mode D2, Generators 1 and 3 showcased opposing oscillations but not in perfect 180-degree phase differences, indicative of an inter-area mode of oscillation. The varied oscillation patterns observed offer a deeper understanding of the complex behaviors and interactions present within the power system, highlighting the significance of detailed examination and interpretation.

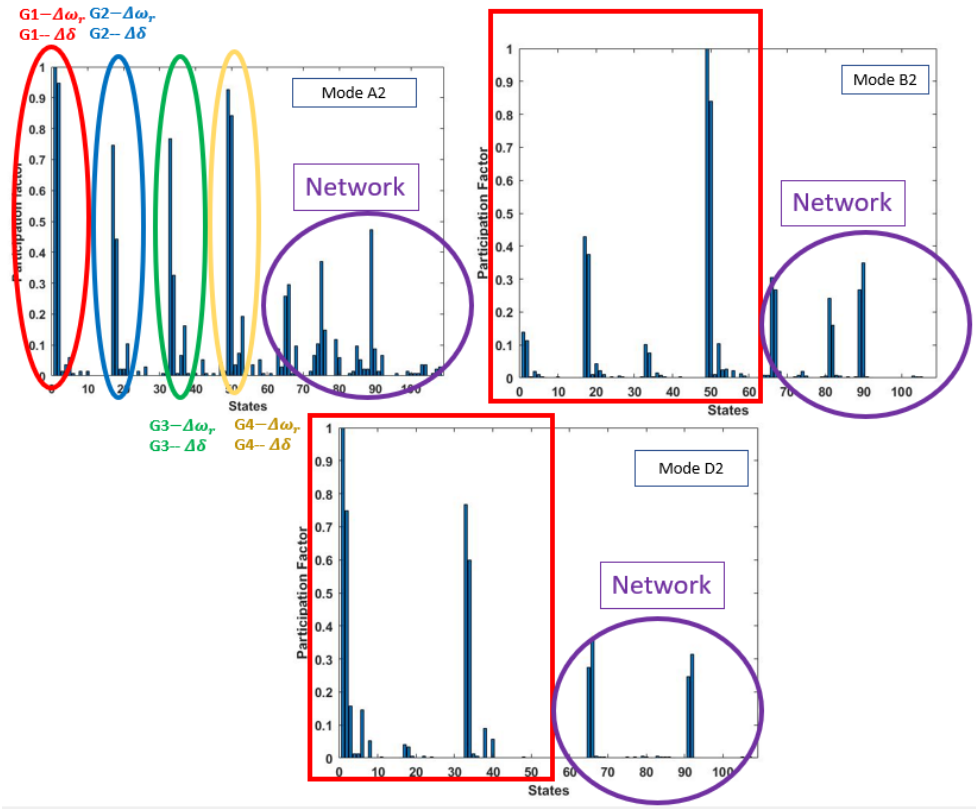

Fig. 3.9. *Participation Factors for modes with lower damping related to scenario 1 mode A, Mode B, Mode D (scenario 2)*

3.2.3 Scenario 3

In scenario three, a wind power plant replaces the conventional power plant which is connected to bus 12 and that wind power plant is in the same capacity as the conventional power plant which is replaced. As observed in the previous scenarios, the system remained stable (all the eigenvalues of the state matrix lie on the left half cycle of the complex plane) with some critical damped modes. However, two additional oscillatory modes with low damping ratios were identified, diverging from the behaviors observed in the earlier scenarios and they were named as mode P and mode Q. Participation factor analysis attributed these modes directly to the wind power plant as shown in the figure 3.11. Specifically, Mode P emerged from the dynamics of the wind turbine's drive train while Mode Q emerged from the DC link and the grid side inverter.

Participation factor analysis 3.11shows that mode P highlights oscillatory behavior with opposing oscillations in θ and ω. This mode revealed a 90-degree phase difference between θ_1 -to-θ_2 and ω_1-to-ω_1 oscillations. This unique behavior suggests complex interactions within the wind turbine's mechanical systems and control mechanisms. Meanwhile, Mode Q is found to be associated with the DC link and states of the grid side inverter. This implies that the control feedback mechanisms within the

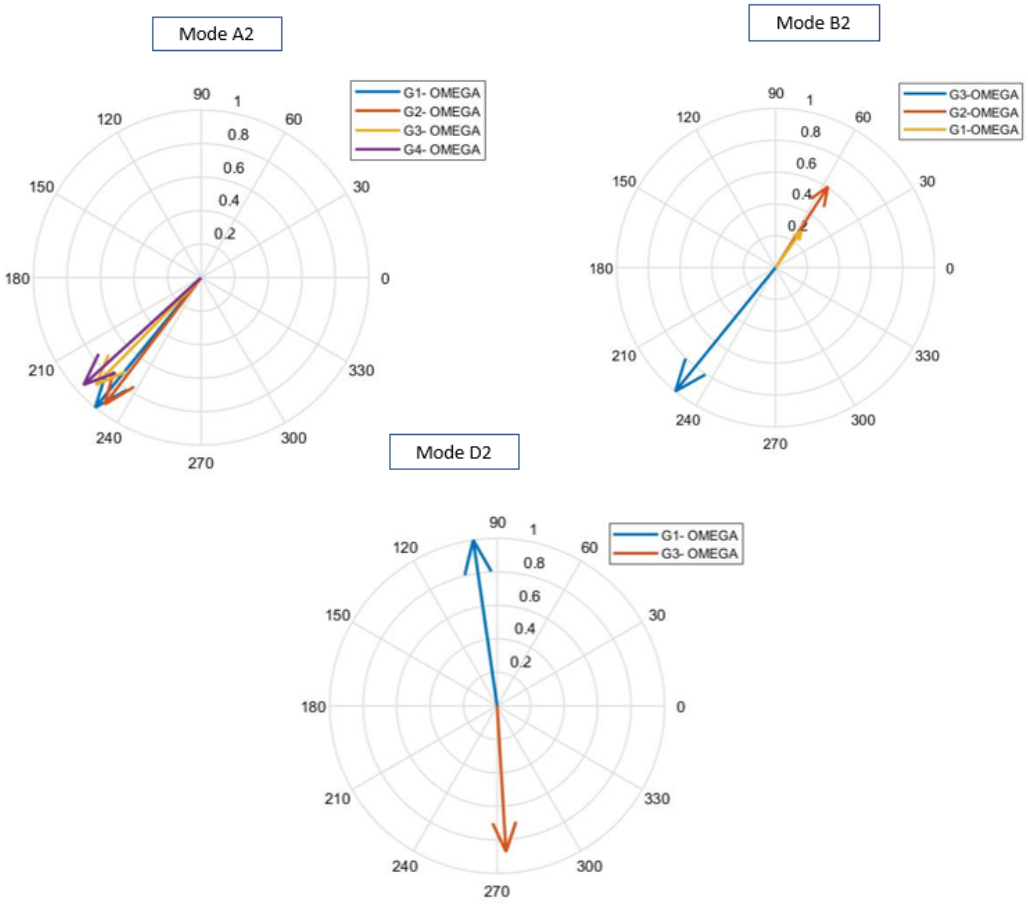

Fig. 3.10. *Mode shape plots for mode A2 , mode B2 , mode D2 (scenario 2)*

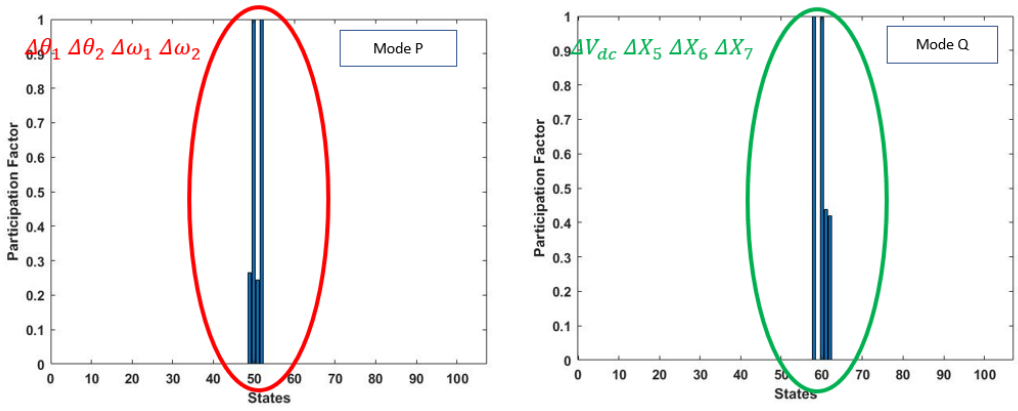

Fig. 3.11. *Participation factors for modes with critical damping from Wind plant (scenario 3)*

inverter may contribute to the dynamics of this mode.

Further examination of the system's dynamic behavior indicated that the damping ratios of some modes experience minor reductions compared to Scenario 2, whereas

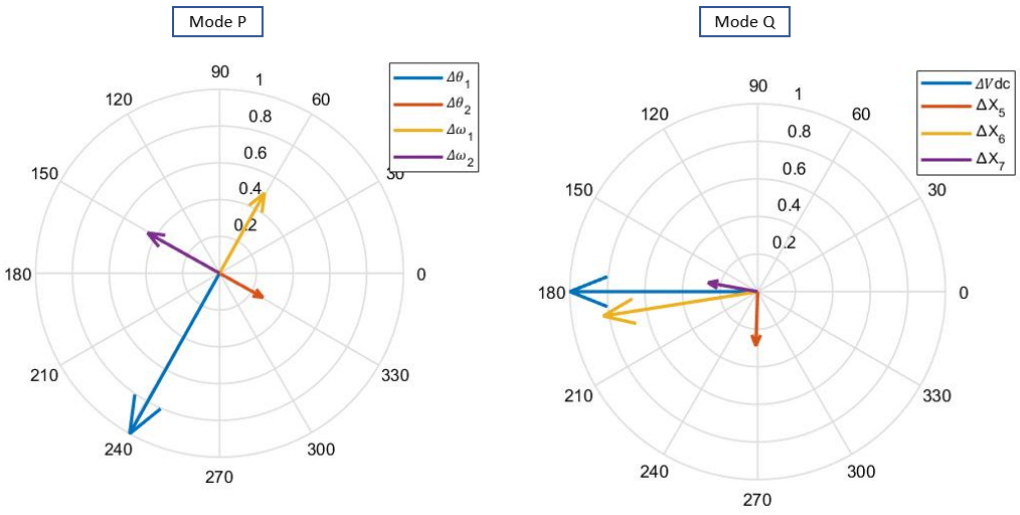

Fig. 3.12. *Mode shape of the modes with critical damping from Wind plant (scenario 3)*

others exhibited slight increments. Collectively, these observations underscore the significant influence of wind power plants on the system's dynamic behavior and stability characteristics. The Table 3.1 clearly shows this fact. In the context of power systems,

Table 3.1
Comparison between the critical modes of Scenario 2 and Scenario 3

Scenario 2				Scenario 3			
Mode	Freq.	D.Ratio	Participating States	Mode	Freq.	D.Ratio	Participating States
E2	2.0777	0.6341	G2, Network	E3	2.0763	0.4776	G2, Network
F2	1.8935	0.9942	G3, Network	F3	1.184	1.0029	G3, Network
G2	1.5607	1.2829	G3, Network	G3	1.035	2.4227	G3, Network
H2	1.1861	1.0968	G4, Network	P	1.9302	0.8245	G4, Network
I2	0.8943	1.8487	G1, Network	I3	1.0125	1.679	G1, Network
				Q	0.154	3.3796	G4, Network

the penetration level of wind energy and its influence on system stability is a paramount concern. Under this research, three wind penetration levels were selected (17%, 25%, and 30%) and examined. By comparing the damping ratios for each penetration level, the impact of integrating wind power into the system stability is identified. As per the results, it is common to see that the damping of the system reduced with the increment of wind penetration. However, the damping ratios associated with modes that have significant participation from wind plants are slightly increased. The table 3.2 shows the behavior of the selected modes that are associated with the previous analysis and their damping ratios with the change of wind penetration.

Table 3.2
Damping Ratios for Different Wind Penetration Levels (scenario 3)

Mode	Penetration 17%	Penetration 25%	Penetration 30%
Mode E3	0.4776	0.4762	0.4759
Mode F3	1.0029	1.0031	1.0022
Mode G3	2.4227	2.4121	2.4112
Mode P	0.8245	0.8286	0.8289
Mode I3	1.016	1.001	1.000
Mode Q	3.3796	3.3825	3.3829

3.2.4 Scenario 4

In Scenario 4, the conventional power plant connected to bus 12 in Scenario 2, is now substituted by a solar power plant of the same capacity. The core difference between Scenario 3 and Scenario 4 lies in the type of renewable energy source integrated. All eigenvalues lie within the left half cycle of the complex plane and it confirms that the system is stable. However, as in the previous scenarios, there are a number of critical oscillatory modes and many of these modes mirror those identified in Scenario 2. From further examination two distinct modes, absent in Scenario 2, have been identified. Through participation factor analysis, these modes are found to stem directly from the dynamics of the solar power plant and are named Mode R and Mode S as shown in 3.13.For instance, Mode R showcased substantial participation from the state variable ΔX_{s1} and the system parameter ΔU_{dc}. This relationship suggests that the dynamics inherent to Mode R are linked to deviations in the DC voltage and potential disturbances within that same voltage domain. On the other hand, Mode S is predominantly influenced by the phase-locked loop (PLL) dynamics, as evidenced by its strong participation from ΔX_{pll} and $\Delta \Theta_{pll}$. This underscores the mode's sensitivity to perturbations in the PLL's state and phase deviations.

Mode shape analysis for mode R and mode S in figure 3.14 shows the relationship between their state variables. For Mode R, the oscillatory behavior between ΔX_{s1} and ΔU_{dc} is notably anti-phase, but not in perfect opposition. Such behavior could imply that as the system deviation in ΔX_{s1} increases, there's a corresponding decrease in ΔU_{dc}, and vice versa, indicating a potential compensatory mechanism between the two. Further examination of the system's dynamic behavior indicated that the damping ratios of some modes experience minor reductions compared to Scenario 2. However, the impact on the damping ratios from the solar power plant is less than the impact from the wind power plant. (But a small number of modes damping ratios experience slide increment also). These observations underscore the significant influence of wind power plants on the system's dynamic behavior and stability characteristics. The Table 3.3 clearly shows this fact.

The integrated level of solar energy in the power system significantly affects the sys-

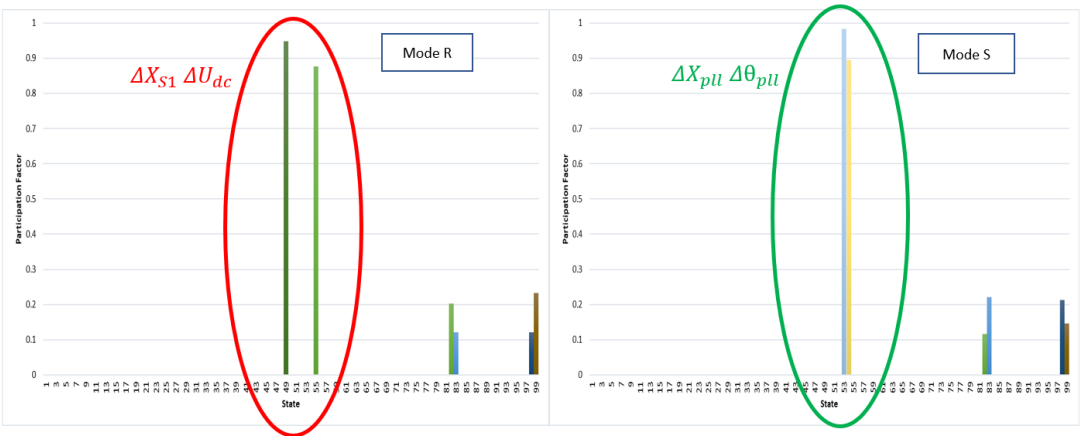

Fig. 3.13. *Participation factors for modes with critical damping from solar plant (scenario 4)*

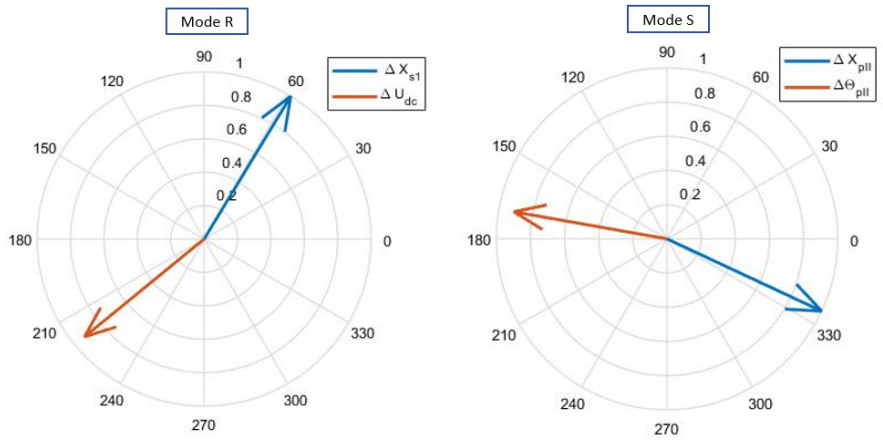

Fig. 3.14. *Mode shapes of modes R and Mode S (scenario 4)*

Table 3.3
Comparison between the critical modes of Scenario 2 and Scenario 4

Scenario 2				Scenario 4			
Mode	Freq.	D.Ratio	Participating States	Mode	Freq.	D.Ratio	Participating States
E2	2.0777	0.6341	G2, Network	E4	2.0736	0.6032	G2, Network
F2	1.8935	0.994	G3, Network	F4	1.891	1.0847	G3, Network
G2	1.5607	1.2829	G3, Network	G4	1.5586	1.2671	G3, Network
H2	1.1861	1.0968	G4, Network	R	0.8998	3.5544	G4, Network
I2	0.8943	1.8487	G1, Network	I4	1.0429	1.8248	G1, Network
				S	0.0589	4.9283	G4, Network

tem's stability and, in this research, three solar penetration levels were analyzed. Here penetration levels are selected as 17%, 25%, and 30% same as analyzed in scenario

3. By evaluating the damping ratios corresponding to each penetration level, insights into the implications of solar power integration on system stability were derived. According to the findings, the general trend was the system's damping decreased with the increment of the solar power level in the system. However, some less amount of modes show a slight increase in their damping with the increment of solar integration. Table 3.4 shows the behavior of the chosen modes in correlation with the prior analysis.Moreover, it was observed that higher potential gain in PLL controllers positively affected the system damping leading to an overall increase in damping.

Table 3.4
Damping Ratios for Different Wind Penetration Levels (scenario 4)

Mode	**Penetration 17%**	**Penetration 25%**	**Penetration 30%**
Mode E4	0.6032	0.6024	0.6019
Mode F4	1.0847	1.0821	1.0818
Mode G4	1.2671	1.2662	1.2660
Mode R	3.5544	3.5538	3.5540
Mode I4	1.8248	1.8241	1.8238
Model S	4.9283	4.9276	4.9281

3.2.5 Scenario 5

In scenario five, both a wind power plant and a solar power plant were simultaneously added to the system as described in the previous chapter. The small signal stability analysis results for this scenario revealed that the systems stability characteristics lay between those observed in scenarios three and four this can be clearly seen in Table 3.5. In this scenario, no specific lower-damped modes were found that interacted exclusively with both the wind and solar power plants. However, it was observed that certain modes exhibited interaction, but with higher damping ratios. The modifications made to the controllers of both the wind and solar power plants have the potential to impact the damping of the system and the interaction of power sources. The changes in controllers, such as adjustments to control gains or control strategies, can influence the response of renewable power plants to disturbances. These modifications may result in changes to the damping ratios of the oscillatory modes and potentially affect the stability of the system.

3.2.6 Scenario 1A

In Scenario 1A's study of the 220kV level Sri Lankan power system, stability is prominently reflected by all eigenvalues residing in the left-hand cycle of the complex plane.

Table 3.5
Comparison between the critical modes of Scenario 2 and Scenario 5

Scenario 2				Scenario 5			
Mode	Freq.	D.Ratio	Participating States	Mode	Freq.	D.Ratio	Participating States
E2	2.0777	0.6341	G2, Network	E4	2.0736	0.6032	G2, Network
F2	1.8935	0.994	G3, Network	F4	1.891	1.0847	G3, Network
G2	1.5607	1.2829	G3, Network	G4	1.5586	1.2671	G3, Network
H2	1.1861	1.0968	G4, Network	R	0.8998	3.5544	G4, Network
I2	0.8943	1.8487	G1, Network	I4	1.0429	1.8248	G1, Network
				S	0.0589	4.9283	G4, Network

This positioning signifies a system that can naturally counteract disturbances. Several oscillatory modes were detected and each of them showed adequate damping while ensuring the system's resilience against potential perturbations and tabulated in table 3.6. Among those modes, four oscillatory modes influenced by different combinations of power plants were identified through mode shape analysis.

Table 3.6
Selected modes in scenario 1A

Mode	Oscilation frequency	Damping Ratio	Participation
M1A-1	0.77	12.1475	Kothmale Upper Kothmale
M1A-2	0.79	13.8686	Kothmale Upper Kothmale Victoria Randenigala Rantambe
M1A-3	0.076	11.2970	Yugadhanavi Lakvijaya
M1A-4	0.63	8.6238	Kelanithissa Yugadhanavi

In Mode M1A-1 analysis, both the Kothmale and Upper Kothmale power plants show significant participation, indicating that they play a dominant role in this mode of oscillation. Interestingly, while both power plants oscillate in the same direction but they are not perfectly aligned as shown in figure 3.15. This coherent movement, even if not 100% aligned, suggests a degree of correlation in their response to this mode of oscillation. Understanding and monitoring this behavior is crucial for power system operators, as it can have implications for system stability and the effectiveness of con-

trol measures designed to mitigate oscillatory disturbances.

In the observed Mode M1A-2 as per the figure 3.16, several power plants, namely

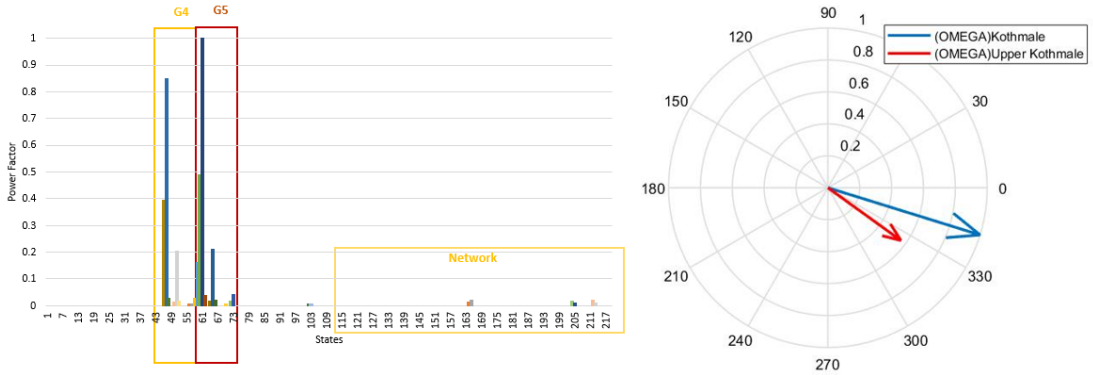

Fig. 3.15. *Particpation factors Mode shapes mode M1A-1 in scenario 1A*

Victoria, Randenigala, Rantambe, Upper Kotmale, and Kotmale, have shown participation. Interestingly, the oscillatory behavior within this mode marked distinct patterns among these power plants. Victoria, Randenigala, and Rantambe power plants oscillate synchronously in the same direction, indicating a coordinated response to system disturbances. In contrast, Kotmale and Upper Kotmale power plants exhibit oscillations in the opposite direction, suggesting that they respond differently within this mode. Such diverse oscillatory behaviors within a single mode underline the complex interplay of forces in the power system.

In Mode M1A-3 analysis, participation is observed from the Lakvijaya and Yugad-

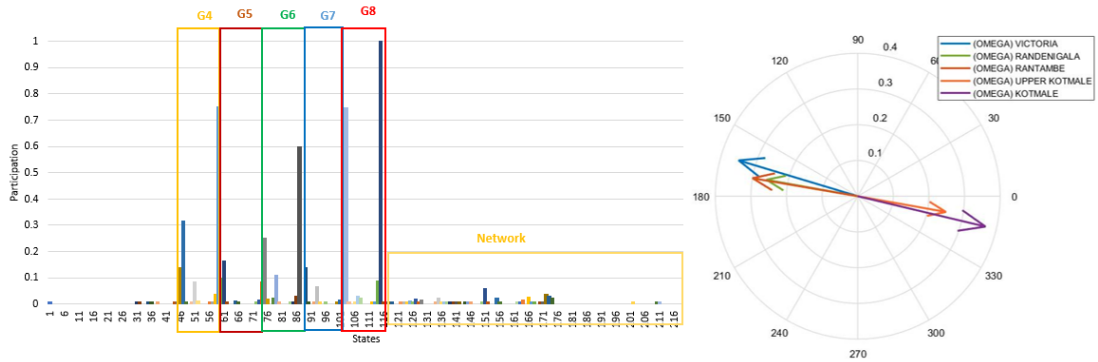

Fig. 3.16. *Particpation factors Mode shapes mode M1A-2 in scenario 1A*

hanavi power plants. Notably, both power plants oscillate coherently in the same direction as shown in figure 3.17. This synchronous behavior indicates that both Lakvijaya and Yugadhanavi are responding similarly to system disturbances within this mode. Such coordinated oscillations highlight the interconnected dynamics between these two power plants.

In Mode M1A-4 analysis, the Yugadanavi and Kelanitissa power plants appear as the

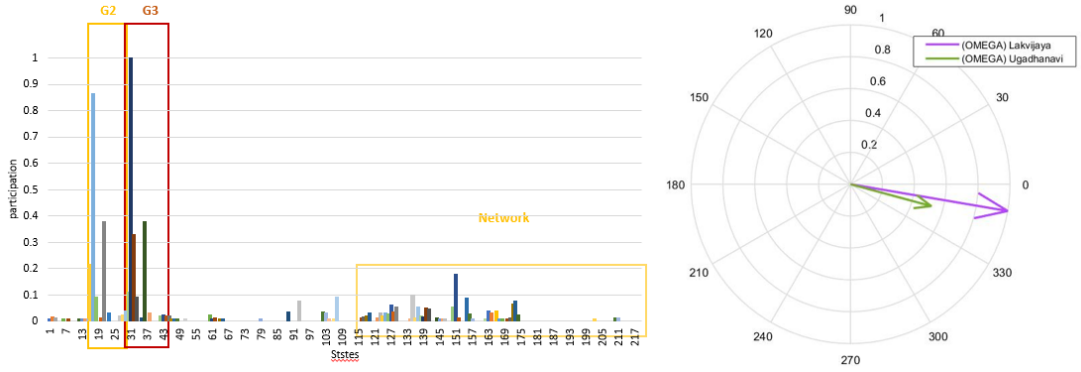

Fig. 3.17. *Particpation factors Mode shapes mode M1A-3 in scenario 1A*

primary participants. these power plants display distinctly antiphase behavior, with their oscillations being 100% opposite in direction As shown in figure 3.18. This counteractive oscillatory pattern suggests that when one plant responds positively to a system disturbance within this mode, the other reacts negatively, and vice versa.

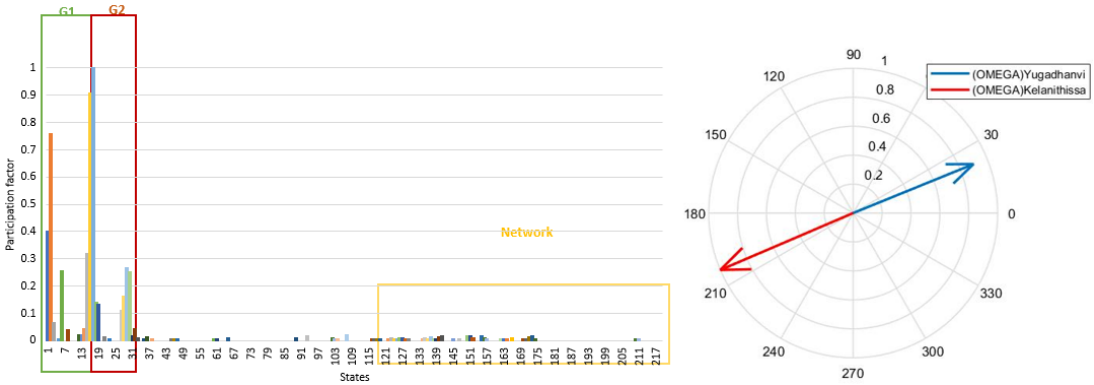

Fig. 3.18. *Particpation factors Mode shapes mode M1A-4 in scenario 1A*

3.2.7 Scenario 2A

In Scenario 2A, a new type of power source was introduced to the power system. Here the aggregate model of the Mannar wind power plant is connected to the 13th bus as previously described. This addition brings about some notable changes to the system's oscillatory behavior by introducing extra oscillations that contribute to the dynamic of the system. Furthermore, this wind integration slightly affects the overall damping characteristics of some other modes. In addition to the modes discussed in the previous scenario, we identify one additional mode with low damping compared to other modes. From participation factor calculation it is identified that this extra mode came from the

Mannar wind power plant. comparison between modes with lower damping compare to other modes in scenario 1A and scenario 2A expresed in bellow table 3.7

Table 3.7
Comparison between the low damping modes of Scenario 1A and Scenario 2A

Scenario 1A				Scenario 2A			
Mode	Freq.	D.Ratio	Participating States	Mode	Freq.	D.Ratio	Participating States
M1A-1	0.77	12.1475	Kothmale Upper Kothmale	M2A-1	0.77	12.06	Kothmale Upper Kothmale
M1A-2	0.79	13.8686	Kothmale Upper Kothmale Victoria Randenigala Rantambe	M2A-2	0.8	13.37	Kothmale Upper Kothmale Victoria Randenigala Rantambe
M1A-3	0.076	11.2970	Yugadhanavi Lakvijaya	M2A-3	0.078	11.06	Yugadhanavi Lakvijaya
M1A-4	0.63	8.6238	Kelanithissa Yugadhanavi	M2A-4	0.671	7.478	Kelanithissa Yugadhanavi
				M2A-5	0.8	5.3087	Mannar Wind

3.2.8 Scenario 3A

In Scenario 3A, the power system model undergoes a significant change. Unlike the previous two scenarios, here the power system is modeled up to 132kV level. This refined granularity leads to some pronounced changes in the system's oscillatory dynamics. This adjustment increased the model complexity compared to the previous scenarios. However, all oscillatory modes now reside in the left half cycle of the complex plane, indicating system stability but the overall damping of the system shows low compared to the 220kV system models and found several under-damped modes and tabulated in the table 3.8.

Table 3.8
Selected under damped modes in scenario 3A

Mode	Oscilation frequency	Damping Ratio	Participation
M3A-1	0.3029	3.5326	Uma oya
M3A-2	0.2885	3.5946	Upper Kothmale
M3A-3	0.2619	3.9536	Victoria
M3A-4	0.2152	1.6556	Lakshapana
M3A-5	0.2023	4.133	Wimalasurendra
M3A-6	0.1023	3.3620	Lakvijaya
M3A-7	0.1832	5.6271	Victoria Randenigala Kothmale Upper Kothmale
M3A-8	0.1786	5.5867	Lakshapana New Lakshapana Canyon

3.2.9 Scenario 4A

In Scenario 4A, the aggregate model of the Mannar wind power plant is connected to the system previously modeled in Scenario 3A. This addition of the Mannar wind power plant to the system affects the overall system dynamics and introduces new oscillatory behaviors to the power system but the whole system maintains stability. However, this modification does bring about two under-damped modes, both originating from the wind power plant itself. The table 3.9 shows the under-damped modes and the participation factors of scenario 4A and compare them with modes of scenario 3A. As per this comparison, damping ratio of some modes slightly reduce with the addition of the wind power plant but some modes damping ratios are showed a slight increase.

Table 3.9
Comparison between the low damping modes of Scenario 3A and Scenario 4A

Scenario 3A				Scenario 4A			
Mode	Freq.	D.Ratio	Participating States	Mode	Freq.	D.Ratio	Participating States
M3A-1	0.3029	3.5326	Uma oya	M4A-1	0.3028	3.5323	Uma oya
M3A-2	0.2885	3.5946	Upper Kothmale	M4A-2	0.2619	3.5911	Upper Kothmale
M3A-3	0.2619	3.9536	Victoria	M4A-3	0.2309	4.7590	Victoria
M3A-4	0.2152	1.6556	Lakshapana	M4A-4	0.2152	1.6556	Lakshapana
M3A-5	0.2023	4.133	Wimalasurendra	M4A-5	0.1591	4.1087	Wimalasurendra
M3A-6	0.1023	3.3620	Lakvijaya	M4A-6	0.1023	3.3620	Lakvijaya
M3A-7	0.1832	5.6271	Victoria Randenigala Kothmale Upper Kothmale	M4A-7	0.1588	4.9066	Victoria Randenigala Kothmale Upper Kothmale
M3A-8	0.1786	5.5867	Lakshapana New Lakshapana Canyon	M4A-8	0.2963	3.2701	Lakshapana New Lakshapana Canyon
				M4A-9	1.5469	1.2675	Mannar Wind
				M4A-10	1.5915	1.3475	Mannar Wind

3.2.10 Chapter Summery

In this chapter, a thorough validation of dynamic power system models was conducted, confirming their authenticity against nonlinear responses from the PSCAD model. Subsequently, through in-depth analyses across multiple scenarios, the implications of integrating conventional and renewable energy sources (wind and solar) were investigated. These observations were made by analyzing eigenvalues, participation factors, and oscillatory modes. This chapter highlighted how the penetration of renewable power influences system stability. Additionally, the Sri Lankan power system case study analyzed the small signal stability of the Sri Lankan power grid and conducted a comparative analysis of how the small signal stability of the system was affected by the addition of the Mannar wind power plant.

CHAPTER 4

CONCLUSIONS

This research investigated the complex state of power system dynamics, providing various significant discoveries and findings. Firstly, the mathematical modeling of the power system which served as the foundation for all subsequent analyses was accomplished accurately. The model wasn't just theoretical. It was thoroughly tested to ensure accuracy and reliability in representing nonlinear responses. The verification of the importance of network dynamics in affecting system stability and the emergence of oscillatory modes is one of this study's notable findings. Network dynamics, which is ignored in constant admittance network modeling, came into play and highlighted how crucial it is to consider the network dynamics when the network is modeled by Dynamic phasor network modeling.

The introduction of renewable energy sources into the power system by replacing conventional power plants poses challenges to the power system stability. When renewable power plants took the place of conventional counterparts, a visible reduction in system damping was observed. Diving deeper into renewables, a comparative analysis between wind and solar integrations brought another layer of understanding. Wind integrations, it was found, exerted a more pronounced impact on system damping than their solar counterparts. However, there were instances where specific modes witnessed slight increments in their damping. Controller configurations emerged as potential game-changers. A notable mention is the impact of higher proportional gains in the PLL controller of solar power plants, which showed a positive effect on damping, although this area is for more comprehensive research.

Further more details were achieved by investigating the variance in penetration levels of renewables. The system's damping exhibited sensitivity to these levels. Predominantly, the effect was negative with increasing renewable penetration, but certain specific modes that relate to the wind power plant reacted positively with the increment of the wind energy in the system. When both wind and solar were integrated, the system's stability profile interestingly settled between the characteristics of scenarios that individually examined these renewable. It showcased the compounded effect of having both energy sources and underlined the need for a balanced energy mix and the delicate balance that needs to be maintained in our pursuit of green energy.

The Sri Lankan power system was accurately modeled using the dynamic phasor approach, revealing the network's intricate dynamics, which significantly contribute to oscillatory modes. The 220kV model shows solid stability without any under-damped oscillatory modes while the modeling up to 132kV shows some underdamped characteristics. However, the overall system shows a stable operation in both models. Furthermore, the integration of the Mannar wind power plant into the system introduces

some extra oscillatory modes and slightly reduces the damping of the system but it does not harm the stability of the system. In conclusion, the Sri Lankan power system can be considered a stable power system. However, all these results are dependent on the accuracy of the data (transmission line data, dynamic data of generators, exciters, governors, and turbines).

In summary, this research path, which involved navigating the complexities of power system dynamics, has established milestones for future initiatives. The results support the idea that, while switching to renewable energy is an ideal goal, it must be approached with careful consideration and preparation to ensure system stability.

REFERENCES

[1] P. Kundur, "Definition and classification of power system stability," *IEEE Transactions on Power Systems*, vol. 19, pp. 1387–1401, 2004.

[2] N. Hatziargyriou *et al.*, "Definition and classification of power system stability – revisited & extended," *IEEE Transactions on Power Systems*, vol. 36, no. 4, pp. 3271–3281, July 2021.

[3] P. S. Kundur and O. P. Malik, "Power system stability and control," 2002.

[4] L. Fernández and J. 24. (2023) Global wind energy share in electricity mix 2022. [Online]. Available: https://www.statista.com/statistics/1302053/global-wind-energy-share-electricity-mix/

[5] R. Moxley, "Wind energy and protection," 2016.

[6] IRENA. (n.d.) Solar energy. [Online]. Available: https://www.irena.org/Energy-Transition/Technology/Solar-energy

[7] Y. C. Y. L. J. Z. Qi JIA, Gangui YAN, "mall-signal stability analysis of photovoltaic generation connected to weak ac grid," *Journal of Modern Power Systems and Clean Energy*, vol. 7, p. 254–267, 2018.

[8] I. subsynchronous working group, "Readers guide to subsynchronous resonance," *IEEE Trans. Power Syst.*, vol. 7, pp. 150–157, 1992.

[9] D. P. S. Gupta, K. R. Padiyar, and M. A. Pai, *Small Signal Analysis of Power systems*. Alpha Science International, 2004.

[10] H. Polinder, W. L. Kling, and J. G. Slootweg, "Dynamic modelling of a wind turbine with doubly fed induction generator," in *Proc. IEEE PowerEng. Soc. Summer Meeting*, 2001, pp. 15–19.

[11] S. Singh, "Study and control of direct driven type-4 grid connected wind energy conversion system," in *2019 5th International Conference on Signal Processing, Computing and Control (ISPCC)*, 2019, pp. 298–305.

[12] R. Kavasseri, Z. L. Miao, C. Zhu, and L. Fan, "Modelling of dfig-based wind farms for ssr analysis," *IEEE Trans. Power Del.*, vol. 25, p. 2073.

[13] C. Karawita and U. D. Annakkage, "Multi-infeed hvdc interaction studies using small signal stability assessment," *IEEE Transactions on Power Delivery*, vol. 24, pp. 910–918, 2009.

[14] S. Jiang, U. D. Annakkage, and A. M. Gole, "A platform for validation of facts models," *IEEE Transactions on Power Delivery*, vol. 21, pp. 484–491, 2006.

APPENDIX A

NETWORK PARAMETERS

A.1 12 Bus System

All the network paramters of the 12 bus system is shows in the follow tables.

Table A.1
Details of Power System Buses

Bus	Bus Type	Nominal Voltage (kV)	Specified Voltage (pu)	Shunt Capacitance (Mvar)	Generation (MW)	Load	
						(MW)	(MVar)
1	PQ	230					
2	PQ	230				280	200
3	PQ	230				320	240
4	PQ	230		160		320	240
5	PQ	230		80		100	60
6	PQ	230		180		440	300
7	PQ	345					
8	PQ	345					
9	Slack	22	1.05				
10	PV	22	1.02		500		
11	PV	22	1.01		200		
12	PV	22	1.02		300		

Table A.2
Power System Line Parameters

From Bus	To Bus	Circuit	R (pu)	X (pu)	B (pu)	Rating (MVA)
1	2	1	0.00920	0.0920	0.178	400
1	6	1	0.02830	0.2767	0.535	250
2	5	1	0.02830	0.2767	0.535	250
3	4	1	0.00920	0.0920	0.178	400
3	4	2	0.00920	0.0920	0.178	400
4	5	1	0.02830	0.2767	0.535	250
4	6	1	0.02830	0.2767	0.535	250
7	8	1	0.00930	0.09250	1.613	500
7	8	2	0.00930	0.09250	1.613	500

Table A.3
Transformer Data (100 MVA base)

From Bus	To Bus	Circuit	R (pu)	X (pu)	B (pu)	Rating (MVA)
1	7	1	0.00000	0.0010	0.000	1000
1	9	1	0.00000	0.0010	0.000	1000
2	10	1	0.00000	0.0010	0.000	1000
3	8	1	0.00000	0.0010	0.000	1000
3	11	1	0.00000	0.0010	0.000	1000
6	12	1	0.00000	0.0020	0.000	500

Table A.4
Power Generation Unit Details

Bus #	Unit #	Area	Generation Type	Installed Capacity (MW)	$P_{\min}$ (MW)	$Q_{\max}$ (MVar)	$Q_{\min}$ (MVar)
9	1	1	Hydro	550	0.0	330.0	-150.0
10	1	1	Hydro	500	0.0	300.0	-100.0
11	1	2	Hydro	400	0.0	240.0	-80.0
12	1	3	Thermal	300	100.0	180.0	-60.0

Table A.5
Details of Shunt Components at Buses

Bus #	Shunt Capacitance (MVar)	Shunt Reactance (MVar)
4	5×40	1×40
5	4×20	1×20
6	6×30	0

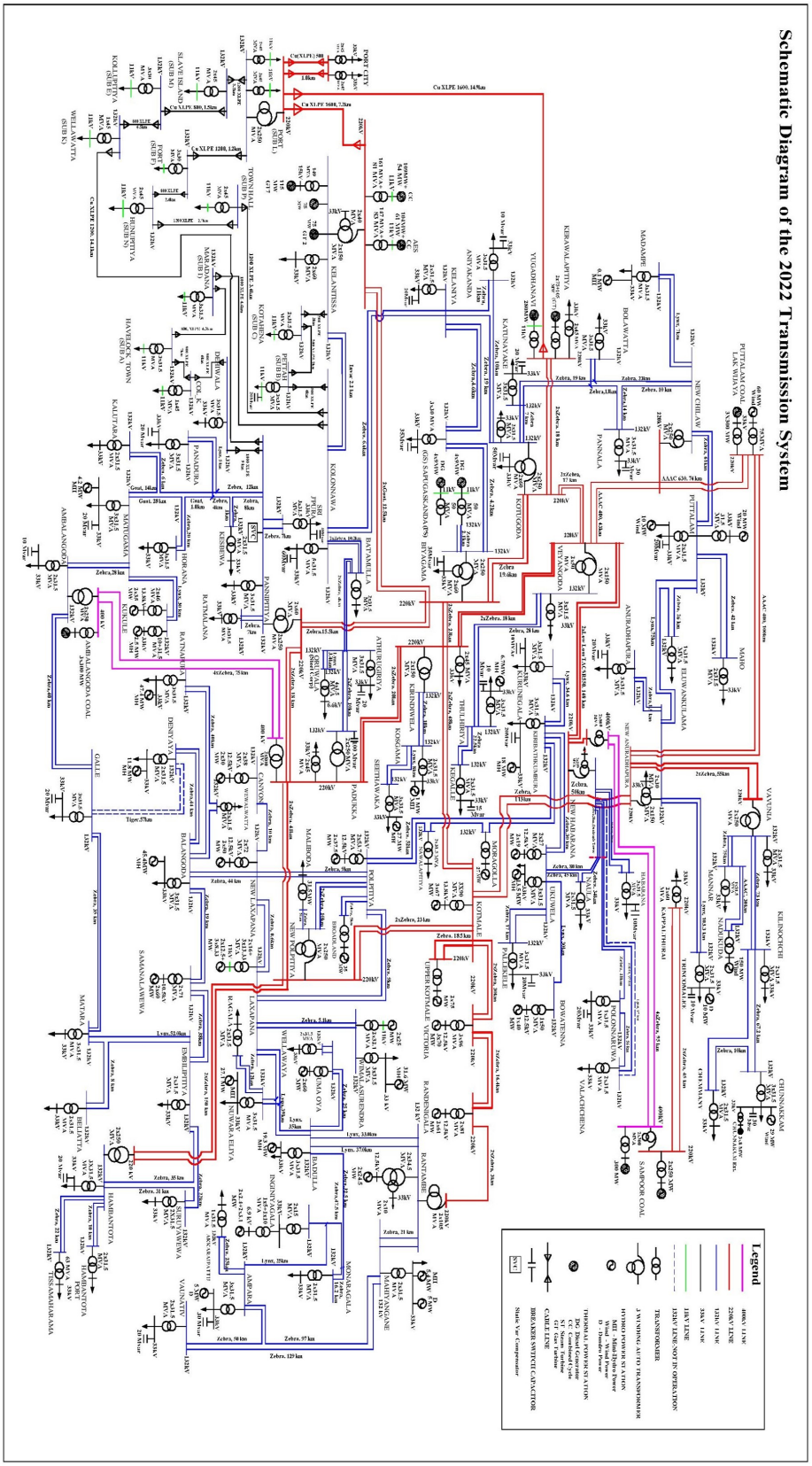

Fig. A.1. *Schematic Diagram of Sri lankan transmission system (CEB Long Term Transmission Development Plan 2013-2022)*

APPENDIX B

POWER PLANT MODELS

B.0.1 Conventional power plant

B.0.1.1 Synchronous generator

The state space model of the 6th order conventional power plant is shown bellow

$$\Delta \dot{X}_g = A_{g1}\Delta X_g + B_{g1}\Delta U_g + E_{g1}\Delta I_g$$

$$\Delta X_g = \begin{bmatrix} \Delta\delta_r & \Delta\omega_r & \Delta\Psi_{fd} & \Delta\Psi_{1d} & \Delta\Psi_{1q} & \Delta\Psi_{2q} \end{bmatrix}^T$$

$$\Delta U_g = \begin{bmatrix} \Delta T_m & \Delta E_{fd} \end{bmatrix}^T$$

$$\Delta I_g = \begin{bmatrix} \Delta I_R & \Delta I_I \end{bmatrix}^T$$

here,

$$\text{A} = \begin{bmatrix} a_{11} & a_{12} & a_{13} & a_{14} & a_{15} & a_{16} \\ a_{21} & a_{22} & a_{23} & a_{24} & a_{25} & a_{26} \\ \vdots & \vdots & \vdots & \vdots & \vdots & \vdots \\ a_{61} & a_{62} & a_{63} & a_{64} & a_{65} & a_{66} \end{bmatrix}$$

$$\text{B} = \begin{bmatrix} b_{11} & b_{12} \\ b_{21} & b_{22} \\ \vdots & \vdots \\ b_{61} & b_{62} \end{bmatrix}$$

$$\text{E} = \begin{bmatrix} e_{11} & e_{12} \\ e_{21} & e_{22} \\ \vdots & \vdots \\ e_{61} & e_{62} \end{bmatrix}$$

$$ag_{12} = \omega_0$$

$$ag_{21} = -\frac{1}{M}\left[i_d e_q - i_q e_d + \left(e_d + 2R_a i_d\right) K_{id1} + \left(e_q + 2R_a i_q\right) K_{iq1}\right]$$

$$ag_{22} = -\frac{K_d}{M}$$

$$ag_{23} = -\frac{1}{M}\left[\left(e_d + 2R_a i_d\right) K_{id3} + \left(e_q + 2R_a i_q\right) K_{iq3}\right]$$

$$ag_{24} = -\frac{1}{M}\left[\left(e_d + 2R_a i_d\right) K_{id4} + \left(e_q + 2R_a i_q\right) K_{iq4}\right]$$

$$ag_{25} = -\frac{1}{M}\left[\left(e_d + 2R_a i_d\right) K_{id5} + \left(e_q + 2R_a i_q\right) K_{iq5}\right]$$
$$ag_{26} = -\frac{1}{M}\left[\left(e_d + 2R_a i_d\right) K_{id6} + \left(e_q + 2R_a i_q\right) K_{iq6}\right]$$
$$ag_{31} = -\frac{\omega_0 R_{fd} L''_{ad}}{L_{fd}} K_{id1}$$
$$ag_{33} = -\frac{\omega_0 R_{fd} L''_{add}}{L_{fd}}\left[\frac{1}{L_{ad}} + \frac{1}{L_{1d}} + K_{id3}\right]$$
$$ag_{34} = -\frac{\omega_0 R_{fd} L''_{add}}{L_{fd}}\left[-\frac{1}{L_{1d}} + K_{id4}\right]$$
$$ag_{35} = -\frac{\omega_0 R_{fd} L''_{add}}{L_{fd}} K_{id5}$$
$$ag_{36} = -\frac{\omega_0 R_{fd} L''_{ad}}{L_{fd}} K_{id6}$$
$$ag_{41} = -\frac{\omega_0 R_{1d} L''_{ad}}{L_{1d}} K_{id1}$$
$$ag_{43} = -\frac{\omega_0 R_{1d} L''_{add}}{L_{1d}}\left[-\frac{1}{L_{1d}} + K_{id3}\right]$$
$$ag_{44} = -\frac{\omega_0 R_{1d} L''_{add}}{L_{1d}}\left[\frac{1}{L_{ad}} + \frac{1}{L_{fd}} + K_{id4}\right]$$
$$ag_{45} = -\frac{\omega_0 R_{1d} L''_{ad}}{L_{1d}} K_{id5}$$
$$ag_{46} = -\frac{\omega_0 R_{1d} L''_{ad}}{L_{1d}} K_{id6}$$
$$ag_{51} = -\frac{\omega_0 R_{1q} L''_{aq}}{L_{1q}} K_{iq1}$$
$$ag_{53} = -\frac{\omega_0 R_{1q} L''_{aq}}{L_{1q}} K_{iq3}$$
$$ag_{54} = -\frac{\omega_0 R_{1q} L''_{aq}}{L_{1q}} K_{iq4}$$
$$ag_{55} = -\frac{\omega_0 R_{1q} L''_{aq}}{L_{1q}}\left[\frac{1}{L_{aq}} + \frac{1}{L_{2q}} + K_{iq5}\right]$$
$$ag_{56} = -\frac{\omega_0 R_{1q} L''_{aq}}{L_{1q}}\left[-\frac{1}{L_{2q}} + K_{iq6}\right]$$
$$ag_{61} = -\frac{\omega_0 R_{2q} L''_{aq}}{L_{2q}} K_{iq1}$$
$$ag_{63} = -\frac{\omega_0 R_{2q} L''_{aq}}{L_{2q}} K_{iq3}$$
$$ag_{64} = -\frac{\omega_0 R_{2q} L''_{aq}}{L_{2q}} K_{iq4}$$

$$ag_{65} = -\frac{\omega_0 R_{2q} L''_{aq}}{L_{2q}} \left[-\frac{1}{L_{1q}} + K_{iq5} \right]$$
$$ag_{66} = -\frac{\omega_0 R_{2q} L''_{aq}}{L_{2q}} \left[\frac{1}{L_{aq}} + \frac{1}{L_{1q}} + K_{iq6} \right]$$

the parameters of B_g matrix as follows

$$bg_{21} = \frac{1}{M}$$
$$bg_{32} = \frac{\omega_0 R_{fd}}{L_{ad}}$$

The parameters of the E_g matrix are given by,

$$eg_{21} = -\frac{1}{M} \left[I_R + (e_d + 2R_a i_d) K_{id7} + (e_q + 2R_a i_q) K_{iq7} \right]$$
$$eg_{22} = -\frac{1}{M} \left[I_I + (e_d + 2R_a i_d) K_{id8} + (e_q + 2R_a i_q) K_{iq8} \right]$$
$$eg_{31} = -\frac{\omega_0 R_{fd} L''_{ad}}{L_{fd}} K_{id7}$$
$$eg_{32} = -\frac{\omega_0 R_{fd} L''_{ad}}{L_{fd}} K_{id8}$$
$$eg_{41} = -\frac{\omega_0 R_{1d} L''_{ad}}{L_{1d}} K_{id7}$$
$$eg_{42} = -\frac{\omega_0 R_{1d} L''_{ad}}{L_{1d}} K_{id8}$$
$$eg_{51} = -\frac{\omega_0 R_{1q} L''_{aq}}{L_{1q}} K_{iq7}$$
$$eg_{52} = -\frac{\omega_0 R_{1q} L''_{aq}}{L_{1q}} K_{iq8}$$
$$eg_{61} = -\frac{\omega_0 R_{2q} L''_{aq}}{L_{2q}} K_{iq7}$$
$$eg_{62} = -\frac{\omega_0 R_{2q} L''_{aq}}{L_{2q}} K_{iq8}$$

all the other parameters of each matrix are zero
d-q axis currents are given by following equations (B.1) and (B.2)

$$\Delta i_d = K_{id1}\Delta\delta + K_{id2}\Delta\omega_r + K_{id3}\Delta\Phi_{fd} + K_{id4}\Delta\Phi_{1d} + K_{id5}\Delta\Phi_{1q} + K_{idd}\Delta\Phi_{2q} + K_{id7}\Delta V_R + K_{ids}\Delta V_I \tag{B.1}$$

$$\begin{aligned}
K_{id1} &= \frac{L''_q e_d - R_{e_e}}{L''_d L''_q + R_q^2} \\
K_{id3} &= \frac{L''_{ds} L''_q}{L_{fd}\left(L''_d L''_q + R_a^2\right)} \\
K_{id5} &= -\frac{L''_{aq} R''_\alpha}{L_{1q}\left(L''_\alpha L''_q + R_\alpha^2\right)} \\
K_{id7} &= -\frac{L''_q \cos(\delta) + R_a \sin(\delta)}{L''_\alpha L''_q + R_a^2}
\end{aligned}$$

$$\begin{aligned}
K_{id2} &= 0 \\
K_{id4} &= \frac{L''_{ad} L''_q}{L_{1d}\left(L''_\alpha L''_q + R_{ag}^2\right)} \\
K_{idb} &= -\frac{L''_{aq} R''_\alpha}{L_{2q}\left(L''_\alpha L''_q + R_a^2\right)} \\
K_{id8} &= -\frac{L''_q \sin(b) - R_a \cos(\delta)}{L''_d L'''_q + R_a^2}
\end{aligned}$$

$$\Delta i_q = K_{iq1}\Delta\delta + K_{iq2}\Delta\omega_r + K_{iq3}\Delta\Phi_{fd} + K_{iq4}\Delta\Phi_{1d} + K_{iq5}\Delta\Phi_{1q} + K_{iq6}\Delta\Phi_{2q} + K_{iq7}\Delta V_R + K_{iq8}\Delta V_I \tag{B.2}$$

$$\begin{aligned}
K_{iq1} &= \frac{R_a e_d + L''_d e_q}{L''_d L''_q + R_\alpha^2} \\
K_{iq2} &= 0 \\
K_{iq3} &= \frac{L''_{ad} R''_d}{L_{fd}\left(L''_d L''_q + R_a^2\right)} \\
K_{iq4} &= \frac{L''_{ad} R''_a}{L'^d_{1d}\left(L''_d L''_q + R_a^2\right)} \\
K_{iq5} &= \frac{L''_a L''_d}{L_{1q}\left(L''_d L''_q + R_a^2\right)}
\end{aligned}$$

$$K_{iq6} = \frac{L''_{aq} L''_d}{L'_{2q}\left(L''_d L''_q + R_a^2\right)}$$
$$K_{iq7} = \frac{L'_d \sin(\delta) - R_a \cos(\delta)}{L''_d L''_q + R_a^2}$$
$$K_{iq8} = -\frac{L'_d \cos(\delta) + R_a \sin(\delta)}{L''_d L''_q + R_a^2}$$

R$_I components of the output current of the generator can be expressas follows$

$$\begin{bmatrix} \Delta I_R \\ \Delta I_I \end{bmatrix} = \begin{bmatrix} cg_{11} & 0 & cg_{13} & cg_{14} & cg_{15} & cg_{16} \\ cg_{21} & 0 & cg_{23} & cg_{24} & cg_{25} & cg_{26} \end{bmatrix} \begin{bmatrix} \Delta\delta \\ \Delta\omega_r \\ \Delta\Phi_{fd} \\ \Delta\Phi_{1d} \\ \Delta\Phi_{1q} \\ \Delta\Phi_{2q} \end{bmatrix} - \begin{bmatrix} yg_{11} & yg_{12} \\ yg_{21} & yg_{22} \end{bmatrix} \begin{bmatrix} \Delta V_R \\ \Delta V_I \end{bmatrix}$$

In the above equation, The parameters of the C_g matrix are given by,

$$cg_{11} = -I_I + \sin(\delta)K_{id1} + \cos(\delta)K_{iq1} \quad cg_{13} = \sin(\delta)K_{id3} + \cos(\delta)K_{iq3}$$
$$cg_{14} = \sin(\delta)K_{id4} + \cos(\delta)K_{iq4} \quad cg_{15} = \sin(\delta)K_{id5} + \cos(\delta)K_{iq5}$$
$$cg_{16} = \sin(\delta)K_{id6} + \cos(\delta)K_{iq6} \quad cg_{21} = I_R - \cos(\delta)K_{id1} + \sin(\delta)K_{iq1}$$
$$cg_{23} = -\cos(\delta)K_{id3} + \sin(\delta)K_{iq3} \quad cg_{24} = -\cos(\delta)K_{id4} + \sin(\delta)K_{iq4}$$
$$cg_{25} = -\cos(\delta)K_{id5} + \sin(\delta)K_{iq5} \quad cg_{26} = -\cos(\delta)K_{id6} + \sin(\delta)K_{iq6}$$

The parameters of the Y_g matrix are given by,

$$yg_{11} = -\sin(\delta)K_{id7} - \cos(\delta)K_{iq7} \quad yg_{12} = -\sin(\delta)K_{id8} - \cos(\delta)K_{iq8}$$
$$yg_{21} = \cos(\delta)K_{id7} - \sin(\delta)K_{iq7} \quad yg_{22} = \cos(\delta)K_{id8} - \sin(\delta)K_{iq8}$$

By considering the stater dynamics 8th order model is developed as follows

$$\Delta\dot{X}_g = A_{g2}\Delta X_g + B_{g2}\Delta U_g + E_{g2}\Delta I_g$$

$$\Delta X_g = \begin{bmatrix}\Delta\delta_r & \Delta\omega_r & \Delta\Psi_d & \Delta\Psi_{fd} & \Delta\Psi_{1d} & \Delta\Psi_q & \Delta\Psi_{1q} & \Delta\Psi_{2q}\end{bmatrix}^T$$

$$\Delta U_g = [\Delta T_m \quad \Delta E_{fd}]^T$$

$$\Delta I_g = [\Delta I_R \quad \Delta I_I]^T$$

here,

$$\mathrm{A}_{g2} = \begin{bmatrix} a_{11b} & a_{12b} & a_{13b} & a_{14b} & a_{15b} & a_{16b} & a_{17b} & a_{18b} \\ a_{21b} & a_{22b} & a_{23b} & a_{24b} & a_{25b} & a_{26b} & a_{27b} & a_{28b} \\ \vdots & \vdots & \vdots & \vdots & \vdots & \vdots & \vdots & \vdots \\ a_{81b} & a_{82b} & a_{83b} & a_{84b} & a_{85b} & a_{86b} & a_{87b} & a_{88b} \end{bmatrix}$$

$$\mathrm{B}_{g2} = \begin{bmatrix} b_{11b} & b_{12b} \\ b_{21b} & b_{22b} \\ \vdots & \vdots \\ b_{81b} & b_{82b} \end{bmatrix}$$

$$\mathrm{E}_{g2} = \begin{bmatrix} e_{11b} & e_{12b} \\ e_{21b} & e_{22b} \\ \vdots & \vdots \\ e_{81b} & e_{82b} \end{bmatrix}$$

The parameters of the A_{g2} matrix are given by,

$$ag_{12b} = \omega_0 \qquad ag_{22b} = -\frac{K_d}{M}$$

$$ag_{23b} = \frac{1}{M}\left[-i_q + \Phi_q K_{id3b}\right] \qquad ag_{24b} = \frac{1}{M}\left[\Phi_q K_{id4b}\right]$$

$$ag_{25b} = \frac{1}{M}\left[\Phi_q K_{id5b}\right] \qquad ag_{26b} = -\frac{1}{M}\left[-i_d + \Phi_d K_{iq6b}\right]$$

$$ag_{27b} = -\frac{1}{M}\left[\Phi_d K_{iq7b}\right] \qquad ag_{28b} = -\frac{1}{M}\left[\Phi_d K_{iq8b}\right]$$

$$ag_{31b} = \omega_0 e_q \qquad ag_{32b} = \omega_0 \Phi_q$$

$$ag_{33b} = \omega_0 R_a K_{id3b} \qquad ag_{34b} = \omega_0 R_a K_{id4b}$$

$$ag_{35b} = \omega_0 R_a K_{id5b} \qquad ag_{36b} = \omega_0$$

$$ag_{43b} = \frac{\omega_0 R_{fd} L_{ppd}}{L_l L_{fd}} \qquad ag_{44b} = -\frac{\omega_0 R_{fd} L_{ppd}}{L_{fd}}\left[\frac{1}{L_l} + \frac{1}{L_{ad}} + \frac{1}{L_{1d}}\right]$$

$$ag_{45b} = \frac{\omega_0 R_{fd} L_{ppd}}{L_{fd} L_{1d}} \qquad ag_{53b} = \frac{\omega_0 R_{1d} L_{ppd}}{L_l L_{1d}}$$

$$ag_{54b} = \frac{\omega_0 R_{1d} L_{ppd}}{L_{fd} L_{1d}} \qquad ag_{55b} = -\frac{\omega_0 R_{1d} L_{ppd}}{L_{1d}} \left[\frac{1}{L_l} + \frac{1}{L_{ad}} + \frac{1}{L_{fd}}\right]$$

$$ag_{61b} = -\omega_0 e_d \qquad ag_{62b} = -\omega_0 \Phi_d$$

$$ag_{63b} = -\omega_0 \qquad ag_{66b} = \omega_0 R_a K_{iq6b}$$

$$ag_{67b} = \omega_0 R_a K_{iq7b} \qquad ag_{68b} = \omega_0 R_a K_{iq8b}$$

$$ag_{76b} = \frac{\omega_0 R_{1q} L_{ppq}}{L_l L_{1q}} \qquad ag_{77b} = -\frac{\omega_0 R_{1q} L_{ppq}}{L_{1q}} \left[\frac{1}{L_l} + \frac{1}{L_{aq}} + \frac{1}{L_{2q}}\right]$$

$$ag_{78b} = \frac{\omega_0 R_{1q} L_{ppq}}{L_{1q} L_{2q}} \qquad ag_{86b} = \frac{\omega_0 R_{2q} L_{ppq}}{L_l L_{1q}}$$

$$ag_{87b} = \frac{\omega_0 R_{2q} L_{ppq}}{L_{1q} L_{2q}} \qquad ag_{88b} = -\frac{\omega_0 R_{2q} L_{ppq}}{L_{2q}} \left[\frac{1}{L_l} + \frac{1}{L_{aq}} + \frac{1}{L_{1q}}\right]$$

The parameters of the B_{g2} matrix are given by,

$$bg_{21b} = \frac{1}{M} \quad bg_{42b} = \frac{\omega_0 R_{fd}}{L_{ad}}$$

The parameters of the E_{g2} matrix are given by,

$$eg_{31b} = \omega_0 \sin(\delta) \quad eg_{32b} = -\omega_0 \cos(\delta)$$
$$eg_{61} = \omega_0 \cos(\delta) \quad eg_{62} = \omega_0 \sin(\delta)$$

d-q axis currents are given by following equations (2.3) and (2.4)

$$.\Delta i_d = K_{id3b} \Delta\Phi_d + K_{id4b} \Delta\Phi_{fd} + K_{id5b} \Delta\Phi_{1d} \tag{2.3}$$

In the above equation,

$$K_{id3b} = -\frac{L_{ad} L_{ppd} \left(L_{fd} + L_{1d}\right)}{L_l L_d L_{fd} L_{1d}} - \frac{1}{L_{dd}}$$
$$K_{id4b} = \frac{L_{ppd}}{L_l L_{fd}}$$
$$K_{id5b} = \frac{L_{ppd}}{L_l L_{1d}}$$

where,

$$L_{ppd} = 1/\left[\frac{1}{L_l} + \frac{1}{L_{ad}} + \frac{1}{L_{fd}} + \frac{1}{L_{1d}}\right].$$

$$\Delta i_q = K_{iq6b} \Delta\Phi_q + K_{iq7b} \Delta\Phi_{1q} + K_{iq8b} \Delta\Phi_{2q} \tag{2.4}$$

In the above equation,

$$K_{iq6b} = -\frac{L_{aq}L_{ppq}\left(L_{1q}+L_{2q}\right)}{L_l L_q L_{1q} L_{2q}} - \frac{1}{L_q}$$
$$K_{iq7b} = \frac{L_{ppq}}{L_l L_{1q}}$$
$$K_{iq8b} = \frac{L_{ppq}}{L_l L_{2q}}$$

where,

$$L_{ppq} = 1/\left[\frac{1}{L_l} + \frac{1}{L_{aq}} + \frac{1}{L_{1q}} + \frac{1}{L_{2q}}\right].$$

R-I components of the output current of the generator can be expressed as follows

$$\begin{bmatrix}\Delta I_R \\ \Delta I_I\end{bmatrix} = \begin{bmatrix} cg_{11b} & 0 & cg_{13b} & cg_{14b} & cg_{15b} & cg_{16b} & cg_{17b} & cg_{18b} \\ cg_{21b} & 0 & cg_{23b} & cg_{24b} & cg_{25b} & cg_{26b} & cg_{27b} & cg_{28b}\end{bmatrix} \begin{bmatrix}\Delta\delta \\ \Delta\omega_r \\ \Delta\Phi_d \\ \Delta\Phi_{fd} \\ \Delta\Phi_{1d} \\ \Delta\Phi_q \\ \Delta\Phi_{1q} \\ \Delta\Phi_{2q}\end{bmatrix}$$

In the above equation, The parameters of the C_{g2} matrix are given by,

$$\begin{aligned}
cg_{11b} &= -I_I & cg_{13b} &= \sin(\delta)K_{id3b} \\
cg_{14b} &= \sin(\delta)K_{id4b} & cg_{15b} &= \sin(\delta)K_{id5b} \\
cg_{16b} &= \cos(\delta)K_{iq6b} & cg_{17b} &= \cos(\delta)K_{iq7b} \\
cg_{18b} &= \cos(\delta)K_{iq8b} & & \\
cg_{21} &= I_R & cg_{23b} &= -\cos(\delta)K_{id3b} \\
cg_{24b} &= -\cos(\delta)K_{id4b} & cg_{25b} &= -\cos(\delta)K_{id5b} \\
cg_{26b} &= \sin(\delta)K_{iq6b} & cg_{27b} &= \sin(\delta)K_{iq7b} \\
cg_{28b} &= \sin(\delta)K_{iq8b} & &
\end{aligned}$$

2.0.1.2 Auxiliary controllers

The parameters related to A_e, B_e, and C_e of the Exciter used in this research, are expressed below:

$$A_e = \begin{bmatrix} ae_{11} & ae_{12} & ae_{13} \\ 0 & ae_{22} & ae_{23} \\ 0 & 0 & ae_{33} \end{bmatrix}$$

$$B_e = \begin{bmatrix} be_{11} \\ be_{21} \\ 0 \end{bmatrix}$$

$$E_e = \begin{bmatrix} 0 & 0 \\ 0 & 0 \\ ee_{31} & ee_{32} \end{bmatrix}$$

Where:

$$ae_{11} = -\frac{1}{T_E}$$
$$ae_{12} = \frac{K_E}{T_E}\left[1 - \frac{T_A}{T_B}\right]$$
$$ae_{13} = -\frac{K_E T_A}{T_E T_B}$$
$$ae_{22} = -\frac{1}{T_B}$$
$$ae_{23} = -\frac{1}{T_B}$$
$$ae_{33} = -\frac{1}{T_1}$$

$$be_{11} = -\frac{K_E T_A}{T_E T_B}$$
$$be_{21} = -\frac{1}{T_B}$$
$$ee_{31} = -\frac{V_R}{T_1|V|}$$
$$ee_{32} = -\frac{V_I}{T_1|V|}$$

The parameters related to A_t, B_t, and C_t of the governor and turbine model used in this research, are expressed below:

$$A_t = \begin{bmatrix} at_{11} & at_{12} & 0 & at_{14} & 0 \\ at_{21} & 0 & 0 & 0 & 0 \\ 0 & at_{32} & at_{33} & 0 & 0 \\ 0 & at_{42} & 0 & at_{44} & 0 \\ 0 & 0 & at_{53} & 0 & at_{55} \end{bmatrix}$$

$$A_t^1 = \begin{bmatrix} a1t_{11} \\ 0 \\ 0 \\ 0 \\ 0 \end{bmatrix}$$

$$B_t = \begin{bmatrix} bt_{11} \\ 0 \\ 0 \\ 0 \\ 0 \end{bmatrix}$$

Where:

$$at_{11} = -\frac{1}{T_p} \qquad at_{33} = -\frac{1}{T_g}$$
$$at_{12} = -\frac{R_t + R_p}{T_p} \qquad at_{42} = \frac{R_T}{T_R}$$
$$at_{14} = \frac{1}{T_p} \qquad at_{44} = -\frac{1}{T_R}$$
$$at_{21} = q \qquad at_{53} = -\frac{2q^2}{T_w G^3}$$
$$at_{32} = \frac{1}{T_g} \qquad at_{55} = -\frac{2q}{T_w}[\frac{1}{G^2} - f_p]$$

$$be_{11} = -\frac{K_E T_A}{T_E T_B} \qquad ee_{31} = -\frac{V_R}{T_1|V|}$$
$$be_{21} = -\frac{1}{T_B} \qquad ee_{32} = -\frac{V_I}{T_1|V|}$$

q is the low rate and G is the gate position

$$a1t_{11} = -\frac{1}{T_p}$$
$$bt_{11} = \frac{1}{T_p}$$

The parameters related toA_m and the value of B_m is shown bellow

$$A_m = \begin{bmatrix} 0 & 0 & ct_{13} & 0 & ct_{15} \end{bmatrix}$$

In here

$$ct_{13} = -\frac{A_t q^2}{G^3}[q - q_{NL}] \qquad ct_{15} = -\frac{A_t}{G^2}[3q^3 - 2q_{NL}q]$$

$$B_m = [-DG - \frac{A_t q^2}{G^2}[q - q_{NL}]]$$

2.0.2 Wind Power plant

The state space model of drive train model's Parameters A_{dt} , B_{dt} are as follows

$$A_{dt} = \begin{bmatrix} 0 & 0 & 1 & 0 \\ 0 & 0 & 0 & 1 \\ \frac{K_{12}}{J_1} & \frac{K_{12}}{J_1} & \frac{-D+D_{12}}{J_1} & \frac{D_{12}}{J_1} \\ \frac{K_{12}}{J_2} & \frac{K_{12}}{J_2} & \frac{D_{12}}{J_2} & \frac{-D+D_{12}}{J_2} \end{bmatrix}$$

$$B_{dt} = \begin{bmatrix} 0 & 0 \\ 0 & 0 \\ \frac{1}{J_1} & 0 \\ 0 & \frac{1}{J_2} \end{bmatrix}$$

The state space model of PMSG's Parameters A_{pm} , B_{pm} are as follows

$$A_{pm} = \begin{bmatrix} -\frac{R_s}{L_{ds}} & \omega_R \\ \omega_r & -\frac{R_s}{L_{qs}} \end{bmatrix}$$

$$B_{pm} = \begin{bmatrix} 1 & 0 & \Psi_{qs0} \\ 1 & 0 & \Psi_{ds0} \end{bmatrix}$$

The state space model of RSC's Parameters A_{rsc} , B_{rsc} are as follows

$$A_{rsc} = \begin{bmatrix} 0 & 0 & 0 \\ K_{im} & 0 & 0 \\ 0 & 0 & 0 \end{bmatrix}$$

$$B_{rsc} = \begin{bmatrix} -i_{ds0} & -i_{qs0} & -V_{ds0} & -V_{qs0} & 1 & 0 \\ -K_{pm} i_{ds0} & -K_{pm} i_{qs0} & -K_{pm} V_{ds0} & -K_{pm} V_{qs0} & K_{pm} & 0 \\ 0 & 0 & 0 & -1 & 0 & 0 \end{bmatrix}$$

The state space model of DC Link Parameters A_{dc} , B_{dc} are as follows

$$A_{dc} = 0$$

$$A_{rsc} = \begin{bmatrix} i_{qg0} & i_{dg0} & V_{qg0} & V_{dg0} & i_{qs0} & i_{ds0} & V_{qs0} & V_{ds0} \end{bmatrix}$$

The state space model of GSC's Parameters A_{dc} , B_{dc} are as follows

$$A_{gsc} = \begin{bmatrix} 0 & 0 & 0 & 0 \\ K_{i3} & 0 & 0 & 0 \\ 0 & 0 & 0 & 0 \\ 0 & 0 & K_{i5} & 0 \end{bmatrix}$$

$$A_{gsc} = \begin{bmatrix} 1 & 0 & -1 & 0 & 0 & 0 & 0 \\ K_{p3} & 0 & -K_{p3} & 0 & 0 & -1 & 0 \\ 0 & 1 & 0 & i_{gq0} & -i_{gs0} & -V_{gq0} & V_{gd0} \\ 0 & K_{p5} & 0 & K_{p5} i_{gp0} & -K_5 V_{gq0} & K_5 V_{gd0} & -1 \end{bmatrix}$$

4.0.3 Solar power plant

The final equation for solar power plant with considering the currrent component in the caonected tx line

$$\boldsymbol{A_{slr}} = \begin{bmatrix} 0 & 0 & 0 & 0 & 0 & 0 & 0 & 0 & 1 \\ k_{i1} & 0 & 0 & 0 & 0 & 0 & -1 & 0 & k_{p1} \\ 0 & 0 & 0 & k_{i5} & 0 & k_{p5}(U_{tq0} - i_{d0} x_g) & 0 & -(1 + k_{p5} x_g) & 0 \\ 0 & 0 & 0 & 0 & 0 & (U_{tq0} - i_{d0} x_g) & 0 & -x_g & 0 \\ 0 & 0 & 0 & 0 & 0 & -(U_{td0} + i_{q0} x_g) & x_g & 0 & 0 \\ 0 & 0 & 0 & 0 & k_{i4} & -k_{p4}(U_{td0} + i_{q0} x_g) & k_{p4} x_g & 0 & 0 \\ \frac{k_{p2} k_{i1}}{L_f} & \frac{k_{i2}}{L_f} & 0 & 0 & 0 & 0 & -\frac{k_{p2}}{L_f} & 0 & \frac{k_{p1} k_{p2}}{L_f} \\ 0 & 0 & \frac{k_{i3}}{L_f} & \frac{k_{p3} k_{i5}}{L_f} & 0 & \frac{k_{p3} k_{p5}(U_{tq0} - i_{d0} x_g)}{L_f} & 0 & -\frac{k_{p3} k_{p5} x_g + k_{p3}}{L_f} & 0 \\ 0 & 0 & 0 & 0 & 0 & t_1 & t_2 & t_3 & t_4 \end{bmatrix}$$